

## Human serum albumin nanoparticles loaded with phthalocyanine dyes for potential use in photodynamic therapy for atherosclerotic plaques

Shubhadeep Banerjee<sup>a,#</sup>, Jayeeta Sengupta<sup>a,#</sup>, Ana Aljarilla<sup>b</sup>, Francesca Setaro<sup>b</sup>, Petri I. Mäkinen<sup>c</sup>, LinPing Wu<sup>d</sup>, Lari Holappa<sup>c</sup>, Andres de la Escosura<sup>b</sup>, Chiara Martinelli<sup>a</sup>, Panagiotis N. Trohopoulos<sup>e</sup>, Seppo Ylä-Herttuala<sup>c</sup>, Rudolf Urbanics<sup>f</sup>, Janos Szebeni<sup>f</sup>, Tomas Torres<sup>b,g,h</sup>, and Silke Krol<sup>i,\*</sup>

<sup>a</sup>FIRC Institute of Molecular Oncology Foundation (IFOM), IFOM-IEO-Campus, via Adamello 16, 20139 Milan, Italy.

<sup>b</sup>Department of Organic Chemistry, Universidad Autonoma de Madrid, 28049-Madrid, Spain

<sup>c</sup>A.I. Virtanen Institute, University of Eastern Finland, Neulaniementie 2, 70210 Kuopio, Finland.

<sup>d</sup>Københavens Universitaet, København, Denmark

<sup>e</sup>CosmoPHOS Ltd, 77 Tsimiski Street, 54622 Thessaloniki, Greece

<sup>f</sup>Semmelweis University, Budapest, Üllői út 78, 1082 Budapest, Hungary

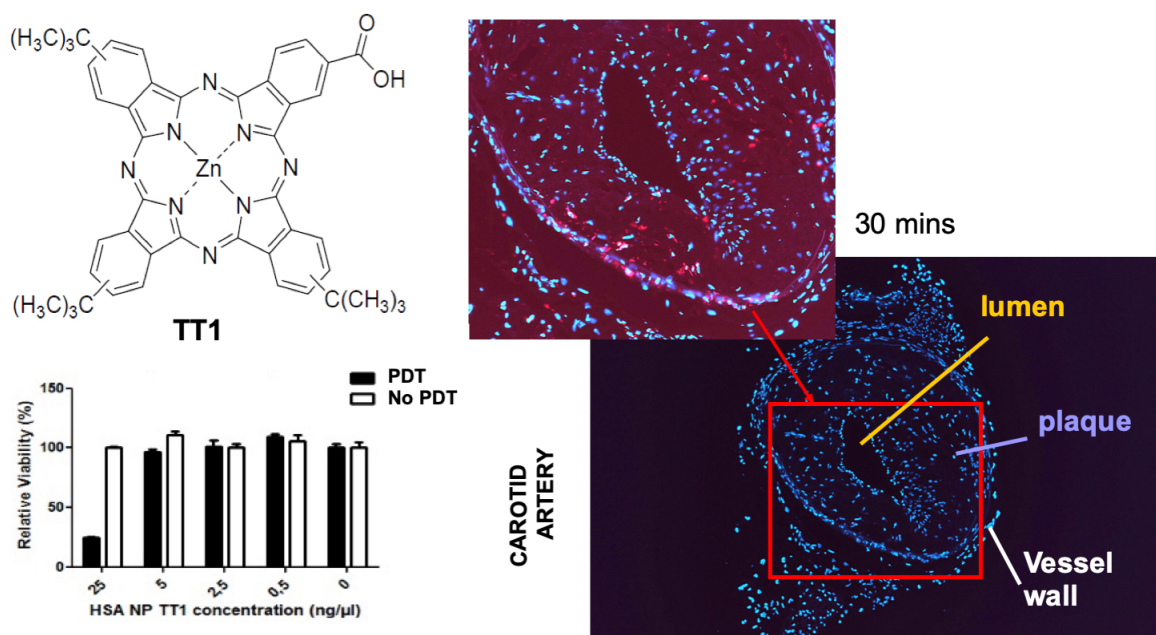
<sup>g</sup>IMDEA Nanoscience, CIUDAD UNIVERSITARIA DE CANTOBLANCO 28049, Madrid, Spain

<sup>h</sup>Institute for Advanced Research in Chemical Sciences (IAChem), Autonoma University of Madrid, Cantoblanco 28049, Madrid, Spain

<sup>i</sup>Laboratory for Nanomedicine, Fondazione IRCCS "Carlo Besta, I IFOM-IEO-Campus, via Adamello 16, 20139 Milan, Italy

#These authors contributed equally to the work.

### Graphical Abstract



\*Corresponding author: Silke Krol, present address: Laboratory for personalized medicine, IRCCS Ospedale Specializzato in Gastroenterologia "Saverio de Bellis", Via Turi 27 - 70013 Castellana Grotte (BA), Italy. Email: [silke.krol@aol.com](mailto:silke.krol@aol.com). phone: +39 080 4994381.

Present addresses: Shubhadeep Banerjee is now with Sun Pharma Advanced Research Company, Vadodara, India. Chiara Martinelli is now with Smart Bio-Interfaces, Istituto Italiano di Tecnologia, Pontedera (Pisa), Italy.

## Abstract

Diseases caused by obstruction or rupture of vulnerable plaques in the arterial walls such as cardiovascular infarction or stroke are the leading cause of death in the world. In the present work, we developed human serum albumin nanoparticles loaded by physisorption with zinc phthalocyanine, TT1, mainly used for industrial application as near-infrared photosensitizer and compared these to HSA NPs loaded with the well-known silicone phthalocyanine (Pc4). The use of NIR light allows for better tissue penetration, while the use of nanoparticles permits high local concentrations. The particles were characterized and tested for toxicity and stability as well as for their potential use as a contrast agent and NIR photosensitizer for photodynamic therapy in cardiovascular disease. We focused on the distribution of the nanoparticles in RAW264.7 macrophage cells and atherosclerotic mice. The nanoparticles had an average size of 120 nm according to dynamic light scattering, good loading capacity for zinc phthalocyanine, and satisfying stability in 50% (v/v) fetal bovine serum for 8 hours and in an aqueous environment at 4°C for 4–6 weeks. Under light irradiation we found a high production of singlet oxygen and the products showed no dark toxicity in vitro with macrophages (the target cells in vulnerable plaques), but at a low  $\mu\text{g/mL}$  nanoparticle concentration killed efficiently the macrophages upon LED illumination. Injection of the contrast agent in atherosclerotic mice led to a visible fluorescence signal of zinc phthalocyanine in the atherosclerotic plaque at 30 minutes and in the lungs with a fast clearance of the nanoparticles. Zinc phthalocyanine loaded human serum albumin nanoparticles present an interesting candidate for the visualization and potentially photodynamic treatment of macrophages in atherosclerotic plaques.

**Keywords:** Photodynamic therapy, cardiovascular disease, phthalocyanine, albumin nanoparticles

### Rationale and Purpose

Diagnostic tools able to identify vulnerable plaques which are more prone to burst than the thicker partially occluding stable plaques in arteriosclerosis are very limited. Vulnerable plaques are prone to rupture easier due to a thin fibrotic flap and macrophages digesting the fibrotic material by the release of metalloproteinases. A contrast agent which allows to visualize preferentially those plaques and reduce the high content of macrophages would be a new therapeutic option which can prevent stroke or cardiac infarction. Photodynamic therapy (PDT) offers the possibility of a very localized treatment of cells which have up taken the drugs and only after activation by invasive light which significantly reduces side-effects. Recently it was shown that PDT had a beneficial effect even for the treatment of cardiovascular disease (CVD). Albumin nanoparticle delivery for the NIR photosensitizer was chosen as because of the good biocompatibility of albumin, expected long half-life time in blood, low expected protein corona, and good loading capacity of albumin for different types of molecules in its native form. A NIR dye will allow the activation by light even in deeper tissue layers.

### Introduction

According to WHO (2017), cardiovascular disease (CVD) along with stroke are the major cause of death (17.9 million per year due to CVD presenting 1/3 of the global death) and disability across the globe for non-communicable diseases with a prevision of an even higher death toll in the future.<sup>1,2</sup>

Myocardial infarction and stroke are induced by an embolus which forms upon rupture of vulnerable atherosclerotic plaques, leading to occlusion and ischemia.<sup>3–5</sup> Atherosclerosis is a slow progressing pathophysiological condition in which lipids and blood-borne material deposits in the form of plaques within the arterial wall.<sup>6</sup> The plaque formation is a complex process involving multiple steps such as the formation and “bursting” of macrophage foam cells (necrosis), extracellular lipid accumulation, loss of structural integrity of smooth muscle cells, solid cholesterol deposition (needle-like crystals), calcification, and hematoma formation and transformation causing chronic inflammation, neovascularization, fibrotic flap disruption, and fibromuscular tissue formation from thrombus.<sup>7,8</sup> Moreover, studies support the important role of cellular processes including mechano-transduction and endothelial cells inflammation, the invasion of macrophages,

and a phenotypic switching of smooth muscle cells in the lesions.<sup>9</sup> Given the manifold events taking place in plaque formation, one can distinguish 2 types of plaques: (i) those stabilized by calcification and (ii) those that are vulnerable that have been destabilized by a thinning of the fibrotic cap due to matrix metalloproteinase digest and macrophage.<sup>5</sup>

The “gold standard” for diagnostics of CVD is angiography. However, one of the limitations of the technique is that it visualizes significant occlusions formed mainly by stable plaques. Another diagnostic tool is the more invasive cardiac catheterization, which gives more detailed information and allows for immediate treatment.<sup>10,11</sup> While techniques do exist to visualize plaques in general, methods to distinguish vulnerable plaques responsible for 70% of the deadly infarctions from stable, calcified plaques are very limited. Therefore, a technology able to identify these plaques in a non-invasive manner and at the same time allow for treatment would be preferred for management of CVD.

PDT is a non-invasive local treatment known as a palliative treatment for non-invasive skin conditions such as basal cell carcinoma and other superficial cancers.<sup>12</sup> Recently, it was studied as a promising treatment option for application in other medical problems such as periodontitis,<sup>13,14</sup> or in gynecology.<sup>15</sup> After the application of a non-toxic photosensitizer, the treated area (dye accumulates in tumor due to enhanced permeation and retention effect) is irradiated with non-toxic preferentially near-infrared (NIR) light (has a better and deeper tissue penetration<sup>12,16</sup>), which activates the photosensitizer. The photosensitizer produces singlet oxygen which damages or kills the target cells selectively. A second mechanism of cell killing is the production of reactive oxygen species by the exposure to the singlet oxygen. This treatment allows for the eradication of the malignant cells without severe side-effects for the body.<sup>17</sup> Increasing evidence indicates the importance of nanoparticulated photosensitizer and PDT for diagnostics and treatment of CVD.<sup>18–21</sup> It was shown that PDT for CVD, named photoangioplasty in clinical trials, can significantly reduce the plaque size.<sup>22,23</sup> The drug diffuses into the plaque in a process which is similar to enhanced permeation, and retention observed in the tumor due to an impairment in

the integrity of the vessel wall either of the lumen from affected vessels or neovascularization of the vasa vasorum.<sup>24</sup>

Frequently used molecules such as NIR-PDT photosensitizers are phthalocyanines (Pc) which have low, dark toxicity but high phototoxicity due to a high yield of singlet oxygen production, strong absorption in the red-NIR region, and fast clearance from the body.<sup>25–29</sup> For example, silicon-based phthalocyanine (Pc4) is a known second-generation photosensitizer, generating singlet oxygen upon photoirradiation with an absorption in the far red at 675 nm and has been used for treating cancer and other diseases.<sup>30–34</sup> Given the additional fluorescence properties of photosensitizers, they can be used both as therapeutics and as diagnostics, sometimes called “theranostics.” One of the drawbacks is that the hydrophobic sensitizer mainly accumulates in the cell membrane therefore killing the cell by necrosis rather than by apoptosis.<sup>33</sup> Necrosis leads to a local inflammation by the release of cytosolic content. Here, a nanoparticle delivery system can increase on one hand the intracellular concentration of hydrophobic drugs and on the other hand, shift the sensitizer entry to an endocytic uptake and hence apoptotic cell death. Nanoparticulated formulation allows changing the biodistribution of the photosensitizer and seems to improve the efficacy of phthalocyanine photosensitizers in PDT.<sup>35</sup> Recently, different nanoparticle delivery systems for PDT in CVD were tested such as micellar preparations<sup>36</sup> or dendrimers.<sup>37,38</sup> While the micellar preparations were not stable enough to confirm the good in vitro data also in vivo experiments<sup>36</sup> the dendrimers were studied only in vitro in a very artificial system.<sup>37</sup>

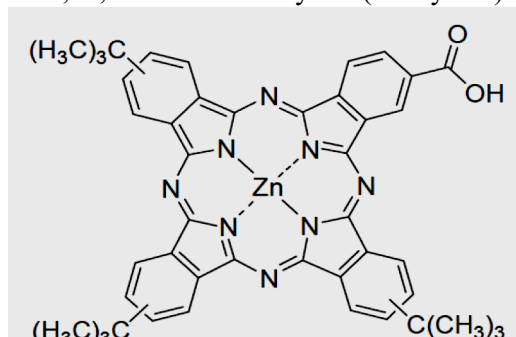
## Experimental

The present work describes the development and characterization of NIR photosensitizer (silicon Pc [Pc4], zinc-based Pc [TT1]) loaded human serum albumin nanoparticles (HSA-NP) and their potential applicability in PDT. The best performing particles were tested for biological performance including macrophage killing efficacy after illumination, immune safety (in vivo in a pig model, and in vitro by complement activation assays on blood) as well as its accumulation in plaques in an

atherosclerotic mouse model as well as off-target organs.

#### Materials and Methods

HSA, non-substituted zinc phthalocyanine (ZnPc), 1,3-diphenylisobenzofuran (DPBF), Eosin Y, 9,10-anthracenediyl-bis(methylene)-



dimalonic acid (ADMA) and dimethyl sulfoxide (DMSO) were purchased from Sigma-Aldrich. Ethanol was purchased from VWR Chemicals, Prolabo (Milan, Italy). All chemicals and solvents were analytical grade and used without further purification.

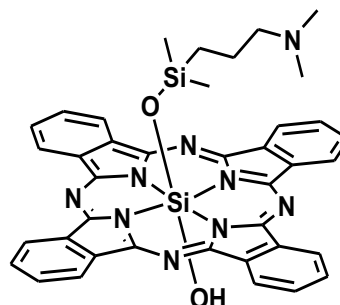


Figure 1. Chemical structure of TT1 (left) and Pc4 (right).

#### Preparation of phthalocyanines

The synthesis of TT1, a photosensitizer originally used for solar cells, was carried as reported in the literature.<sup>39,40</sup> In brief, the synthesis initiated with a statistical condensation of 4-tert-butylphthalonitrile and 4-hydroxymethylphthalonitrile (in a 4:1 ratio), in the presence of zinc acetate as metal salt and refluxing dimethylaminoethanol (DMAE) as a solvent. From the obtained hydroxymethyl-Pc, 2 successive oxidation steps with pyridine-SO<sub>3</sub> complex and NaClO<sub>2</sub>/H<sub>3</sub>NO<sub>3</sub>S lead to the final product TT1 (Figure 1 left). A detailed physicochemical characterization of TT1 can be found in Cid et al.<sup>35</sup>

The synthesis of Pc4 (Figure 1 right) was carried out adapting procedures from literature.<sup>41,42</sup> In particular, the reaction between silicon phthalocyanine (SiPc) dihydroxide (SiPc(OH)<sub>2</sub>) and 3-(methoxydimethylsilyl)-N,N-dimethylpropan-1-amine in distilling pyridine yields a SiPc derivative with 2 di-methylaminopropylsiloxy axial substituents. The selective displacement of one of these substituents with trichloroacetate and the subsequent substitution of the latter with an OH ligand allows obtaining Pc4 in an overall yield of 70%.

#### Synthesis of Pc-loaded HSA-NPs

Empty HSA nanoparticles were prepared by a modified desolvation technique first described by Langer et al.<sup>43</sup> For this, 8.0 mL absolute ethanol was added at a rate of 1mL/min under continuous stirring (500 rpm) at room

temperature to 200 mg HSA dissolved in 2.0 mL of 10 mM NaCl solution (pH=8.10). Then 0.8% (v/v) glutaraldehyde in water (5.88 μL) was added to induce particle cross-linking and the suspension was stirred for 24 hours at room temperature. NPs were collected and washed by centrifugation (16595 × g) for 15 minutes at 20°C and resuspension in ethanol followed by sonication for 15 minutes (repeated twice). Finally, the supernatant was removed, and the NPs were dried in a desiccator for 48 hours. The HSA-NPs were stored as a dry powder at RT upon use. In order to study the influence of different desolvation agents and volumes as well as the speed of desolvation addition on the particle size and dispersity index, smaller test batches were prepared with ¼ of the described volumes (Table S1).

For the preparation of HSA-Pc4 and HSA-TT1 NPs, 100 mg of HSA was dissolved in 2 mL of 10 mM NaCl (pH=8.10). Predetermined volumes of the stock solution of the respective dyes in DMSO were added to the HSA solution and the mixtures were incubated in dark for 2 hours with occasional vortex. The ratio of the dyes to the HSA varied from 1:10 to 1:20 for various formulations (10, 20, 40, 80, 120, 160 μL). Cross-linking and NP purification followed the same procedure described for empty HSA-NPs. Washing steps were repeated until a colorless supernatant was obtained. The supernatants were pooled in order to determine the dye entrapment.



### *Encapsulation efficiency*

Powdered NPs were dissolved in phosphate-buffered saline (PBS) to a concentration of 1 mg/mL. The entrapment efficiency and yield were determined with UV-Vis spectroscopy using Ultraspec 2100 pro (Amersham Biosciences, US). The dry weight of the nanoparticles was measured. The yield of the nanoparticle synthesis was calculated<sup>44</sup> by the formula:

$$\% \text{ NP Yield} = (\text{Weight of NPs obtained} / [\text{weight of dye} + \text{weight of HSA used for NPs synthesis}]) \times 100$$

The protein content of the obtained NPs was calculated using Bradford assay according to the protocol provided by the manufacturer. Briefly, 10  $\mu$ L of HSA-NPs (1 mg/mL) were added into 990  $\mu$ L of diluted Bradford reagent and incubated at RT for 20 minutes. The absorbance was measured at 595 nm and the HSA concentration of the NPs was calculated by means of an HSA standard curve.

During the synthesis of the nanoparticles, the number of dyes in the supernatant after each step of centrifugation was quantified to calculate the entrapment efficiency of the respective dyes in the nanoparticles. A standard curve was plotted before using standard concentrations of dye dissolved in DMSO. The spectrophotometric quantification was done by measuring the absorbance at 672 and 680 nm for Pc4 and TT1, respectively. The percentage of encapsulated dye was calculated using:

$$\% \text{Entrapment} = (1 - [\text{Free dye concentration} / \text{Initial dye concentration}]) \times 100$$

### *Physicochemical characterization*

#### *Dynamic light scattering analysis and zeta potential*

Immediately before use, the Pc-loaded HSA-NPs were dissolved in water to concentrations of 6.96  $\mu$ M Pc4 and 7.5 nM HSA and 6.37  $\mu$ M TT1 and 7.5 nM HSA respectively. The diameter, size distribution, and electrophoretic mobility of HSA, HSA-Pc4 and HSA-TT1 NPs were measured by (DLS) using Nano ZS (Malvern, UK). In order to use the recommended attenuator settings of 7-9, the NPs were diluted for the DLS measurement. The zeta potential was obtained by a further 10-fold dilution in Milli-Q grade water of the DLS sample to reduce the back scattering since the

measurement was not performed at 173° NIBS as for DLS.

### *Nanoparticle tracking analysis*

The size and concentration of HSA-TT1 NPs were analyzed by nanoparticle tracking analysis (NTA) using an LM-10 (NanoSight, Malvern Instruments, Malvern, UK). The particles for NTA had a ratio of 1:10 (dye:HSA). Measurements on appropriately diluted NPs in PBS were performed in triplicates of 60-second video captures with camera level 11 and detection threshold 5. The data were analyzed using software version 3.0.

### *UV-Vis*

The fluorescence emission spectra of the Pc-loaded NPs were measured by UV-Vis using an LS 55 Luminescence spectrofluorometer (Perkin Elmer, USA). For this measurement NPs were dissolved in water and measured at an excitation wavelength of 670 nm for TT1-HSA and  $\lambda_{\text{ex}}=680$  nm for Pc4-HSA NPs respectively.

### *Negative stain high-resolution transmission electron microscopy and energy dispersive spectroscopy*

10  $\mu$ L of the samples (1 mg/mL in distilled water) were deposited on a 300-mesh copper grid coated with carbon (Electron Microscopy Sciences, USA). After 1 minute, the excess sample was removed and a drop of 2% (w/v) ammonium molybdate was placed on the grids to negative stain the HSA-NPs. The excess negative stain was removed, and the grids were air-dried. The morphology of the nanoparticles was observed using a transmission electron microscope (TEM) JEM-2100 HRTEM (JEOL, Japan) along with energy dispersive spectroscopy (EDS) detector in bright field mode under an operating voltage of 200 kV. The elementary analysis by EDS was performed to confirm the presence of Zn and Si in the phthalocyanine-loaded HSA-NPs.

### *Attenuated total internal reflection - Fourier Transform Infrared Spectroscopy (ATR-FT-IR)*

200  $\mu$ L of the Pc dye-loaded HSA-NPs were added on the surface of zinc selenide (ZnSe) ATR crystal as described previously<sup>45</sup> to obtain a uniform film on the crystal. The experiments were performed in Nexus-870 FTIR spectrometer (Thermo Nicolet Corporation, USA) by scanning in the infrared

region of 4000 – 800 cm<sup>-1</sup>. The data obtained was analyzed using the OMNIC software (version 6.0 A) bundled with the instrument. Background spectra measured with the blank ZnSe crystal were subtracted from the individual spectrum. Fourier Transform Infrared Spectroscopy was employed to study possible interactions and bonding patterns between the Pc4 dye and HSA.

#### *Determination of Singlet Oxygen Quantum Yield*

As some of the photosensitizers showed significant quenching in an aqueous environment it was necessary to determine the quantum yield both in water and DMSO.

##### *Yield in DMSO*

Singlet oxygen quantum yields ( $\Phi\Delta$ ) of Pc4 and TT1 dye, HSA, HSA-Pc4 and HSA-TT1 NPs were measured in DMSO, following a procedure reported by Wohrle et al.<sup>46</sup> based on the photo-induced decomposition of the chemical trap 1,3-diphenylisobenzofuran (DPBF). Non-substituted ZnPc was used as reference compound ( $\Phi\Delta(\text{DMSO}) = 0.67$ ).<sup>47</sup> A 2 mL stock solution of DPBF (with an absorbance of ca. 1) in DMSO was taken in a 1 × 1 cm quartz optical cell and kept for 1 minute. A concentrated stock solution of ZnPc in DMSO was then added, in a defined amount to reach an absorbance of the final solution in the Q-band maximum of about 0.1. The solution was stirred and irradiated for defined time intervals using a halogen lamp of 300 W. The incident light was filtered through a water filter and an orange HOYA G filter to remove heat and light under 530 nm, respectively. The decrease of DPBF concentration in DMSO solution with irradiation time was monitored at 417 nm in a UV-Vis spectrophotometer. The data was plotted for further calculations.

##### *Yield in water*

The singlet oxygen quantum yields ( $\Phi\Delta$ ) of HSA, HSA-Pc4 and HSA-TT1 NPs were measured in H<sub>2</sub>O as reported earlier based on the photo-induced decomposition of the chemical trap  $\alpha,\alpha'$ -(anthracene-9,10-diyl)-dimethyl-malonic acid (ADMA). Eosin Y was used as reference compound ( $\Phi\Delta(\text{H}_2\text{O})=0.60$ )<sup>65</sup> Experimental measurements were carried out as mentioned before, with a few modifications. Incident light was filtered through a water filter and an MS filter to remove heat and light under

455 nm, respectively. Decrease of ADMA concentration in H<sub>2</sub>O solution with irradiation time was monitored at 380 nm in a UV Vis spectrophotometer. Data obtained were plotted and calculations were done in order to get the singlet oxygen quantum yield.

#### *Stability study of HSA-Pc4 and HSA-TT1 NPs*

##### *Serum stability*

A stock solution was prepared by suspending the NPs with and without photosensitizer in deionized water to a concentration of 1 mg mL<sup>-1</sup>. Next, nanoparticles (Pc4-HSA and TT1-HSA) were added to 50% (v/v) FBS or to a physiological saline solution on a thermoshaker for up to 24 hours at room temperature. An aliquot of the NPs was collected at predetermined time points of 2, 4, 8, and 24 hours to determine the amount of released dye and NP size. NPs were centrifuged at 12500 rpm (16595 × g) for 15 minutes at 20°C and the supernatant was collected and analyzed with a spectrophotometer to calculate the release dye percentage.

##### *Stability of NP solution*

The NPs as prepared were suspended in deionized water at a concentration of 1 mg/mL to form a stock solution and stored at 4°C for up to 6 weeks. Every week the NP size distribution and zeta potential were calculated using DLS. In order to determine the amount of released dye, the NPs were centrifuged for 15 minutes at 16595 × g and the supernatant was analyzed in UV-Vis spectrophotometer to determine the amount of released dye.

##### *In vitro experiments*

Murine macrophages RAW264.7 were grown in Dulbecco's modified Eagle's Medium (Gibco) supplemented with 10% heat inactivated FBS, L-glutamine (2 mM), 1% non-essential amino acids, 1% sodium pyruvate, penicillin (100 U mL<sup>-1</sup>), streptomycin (100 µg mL<sup>-1</sup>). Cultures were incubated at 37°C, 5% CO<sub>2</sub> and passaged regularly when reaching 70–80% confluence.

HSA-NPs with and without photosensitizer dye were sonicated (Bandelin, Sonorex) for 15 minutes prior to cell incubation. The complete absence of free dye from the loaded NPs was tested according to the protocol reported by Andreozzi et al.<sup>48</sup> Cell membranes were stained with Cell Mask™ Green (Life Technologies,

Monza, Italy), following the manufacturer's instructions. Cellular uptake and internalization of labeled NPs was visualized by using an inverted confocal laser scanning microscope (Leica TCS SP5) equipped with 488 and 633 nm laser lines.

#### *In vitro cell killing and dark toxicity*

Murine macrophages RAW264.7 were grown in Dulbecco's modified Eagle's Medium (Gibco) supplemented with 10% heat inactivated FBS, L-glutamine (2 mM), 1% non-essential amino acids, 1% sodium pyruvate, penicillin (100 U mL<sup>-1</sup>), streptomycin (100 µg mL<sup>-1</sup>). Cultures were incubated at 37°C, 5% CO<sub>2</sub> and passaged regularly when reaching 70–80% confluence.

HSA-NPs with and without photosensitizer dye were sonicated (Bandelin, Sonorex) for 15 minutes prior to cell incubation. The complete absence of free dye from the loaded NPs was tested according to the protocol reported by Andreozzi et al.<sup>44</sup>

The cell-killing efficacy as well as the dark toxicity of HSA-NPs was analyzed on RAW264.7 cells using MTS assay (Promega, Milan, Italy). In this assay, cells seeded into a 96-well plate. After 24 hours, HSA-NPs were added to the cells in escalating doses, and the cells were incubated for another 24 hours. The cells were illuminated with a custom-made LED device emitting light at 670 nm wavelength for 10 minutes, with LED light intensity of 3.04 mW/cm<sup>2</sup>. Twenty-four hours later, MTS reagent was added to the cells for 1 hour and the resulting signal was analyzed by spectrophotometry (Multiskan Ascent, MTX LabSystems, Florida, USA). Cells without nanoparticles were used as a control, as well as solutions containing only the nanoparticles but no cells. The dark toxicity of the compounds was analyzed without LED light illumination.

#### *In vitro complement activation assays*

Details for human serum preparation, characterization and functional assessment of complement pathways were in accordance with our previous studies.<sup>49,50</sup> To measure complement activation *in vitro*, we determined the NP-induced rise of human serum complement products C5a and sC5b-9 using the respective ELISA kits (Quidel, San Diego, CA, USA) according to the manufacturer's protocols as described previously.<sup>45,46</sup> Briefly,

complement activation was initiated by adding the required quantity of TT1 loaded HSA-NPs to undiluted serum in Eppendorf tubes in a shaking water bath at 37°C for 30 minutes, unless stated otherwise. Reactions were terminated by quickly cooling samples on ice and adding 25 mM ethylenediaminetetraacetic acid (EDTA). After centrifugation, the supernatant was used for the determination and quantification of complement activation products C5a and sC5b-9. Control serum incubation contained PBS (the same volume as the NP samples) to assess background levels, and zymosan (1 mg/mL) was used as a positive control for monitoring complement activation throughout. Sera from 3 individuals were tested separately and each incubation was performed in triplicates.

#### *Nanoparticle administration in vivo*

##### *Pig model*

Three young male pigs of 21, 21, and 24 kg were used for *in vivo* administration of TT1-HSA-NPs. The animals were purchased from approved experimental animal vendors. They remained in quarantine for 5 days prior to the experiments. The closed chest *in vivo* pig experiment was performed on anesthetized pigs. Animals were sedated by intramuscular injection of Calypsol/Xilazine (2–4/1.5–2 mL, based on body weight) injections in the stalls to avoid stress, and were transported sedated to the operating room. The anesthesia was maintained using isoflurane inhalation narcosis (2–3%) with oxygen. The pigs were instrumented with Swan-Ganz catheter (Ref. No.: AI-07124, 5 Fr. 110 cm, ARROW INTERNAT. INC.), introduced into the pulmonary artery through the right external jugular vein → right atrium → right ventricle. The pulmonary arterial pressure (PAP) was monitored using a pressure transducer, and a second pressure transducer was connected to the cannula in the left femoral artery to record the systemic arterial pressure (SAP). The left femoral vein was cannulated for blood sampling (for blood cell counts and for TxB2 measurements) and the left external jugular vein was cannulated for fluid supply and administration of control and test materials. All incision areas were shaved and disinfected by a liberal application of povidone-iodine 10% and closed by suture after fixation of cannulas. PAP, SAP, heart rate (HR), and

electrocardiography were continuously monitored and recorded by ADInstruments LabChart Pro v8 model and software. Other details of surgery, instrumentation and hemodynamic analysis were described in the original studies.<sup>51,52</sup>

### Testing procedure

Baseline blood samples were taken, and the physiological parameters were recorded for 15 minutes before the first injection of the test material. Initially pig 1 and pig 2 were injected with previously prepared TT1-HSA-NPs (2.5 mg in 20 mL (=0.125 mg NP/mL for 0.1 mg/kg) and 25 mg in 20 mL (1.25 mg NP/mL for 1 mg/kg).

For experiments with the highly concentrated NP solutions, the sample was prepared fresh from lyophilized dry powder by dilution in saline to the final concentration of 300 mg in 20 mL (=15 mg NP/mL) for an injection of 10 mg NPs/kg weight per pig (pig 3). From this stock solution, the concentrations of 1 mg/kg and 0.1 mg/kg pig were prepared. The respective suspensions were bolus injected into the left external jugular vein. Boluses were flushed into the circulation with an additional 5 mL of saline solution. The complete test involved quantitation of the cardiopulmonary, hemodynamic, skin, hematologic and blood chemical changes.

### Atherosclerotic mouse model

For biodistribution study, 11-month-old male LDLR<sup>-/-</sup>/ApoB100/100 - mice were used at different time points (30 minutes, 3 hours, and 24 hours). Mice were fed on Western type diet TD 88137 Harlan Teklad, 42% calories from fat and 0,15% from cholesterol, Envigo) diet for 7 months. Diet and water were provided ad libitum. The NPs were dissolved from dry powder and TT1-HSA-NPs were injected via tail vein to a final concentration of 1 mg NPs/kg weight per mouse. All animal procedures were approved by The Animal Experiment Board in Finland and carried out in accordance with the guidelines of the Experimental Animal Committee of the University of Eastern Finland.

## Results and Discussion

### Preparation and characterization of the Pc-loaded HSA-NPs

Experiments to optimize the preparation conditions for the nanoparticles were performed by varying the desolvation solvent and the speed by which the solvent/mixture was added to the HSA solution (Table S1). We observed that the composition of the desolvation agents as the added volume has some limited influence on the particle size as well as on the polydispersity index (Table S1). Summarizing the results, we determined that the smallest HSA-NPs with the lowest polydispersity index (PDI) of particles were prepared with 6:2=acetone/water. Additionally, we found that slow desolvant addition in the presence of the photosensitizer TT1 led to 2 peaks in all preparations except for using pure ethanol (data not shown). Therefore, we continued the preparation with ethanol as a desolvation agent because of its lower toxicity.

The Pc (TT1, Pc4) loaded HSA-NPs were prepared with different photosensitizer concentrations and the resulting nanoparticles were characterized for their size (DLS), surface charge (zeta potential), entrapment efficiency, and singlet oxygen production (Table S2). The singlet oxygen quantum yield was determined in order to evaluate a potential efficacy for PDT. For the free Pc4 and TT1 dyes in DMSO, the yield was calculated to be 0.227 and 0.353 respectively, while for the HSA NP the yield was 0.014 for Pc4 and 0.016 for TT1 in water. The significant lower singlet oxygen yield of Pc bound to the HSA NP was explained due to quenching of the photosensitizer in the presence of water as compared to DMSO and the interaction of the produced singlet oxygen with the HSA. (Table S2).

Fluorescence absorbance and fluorescence emission intensity detected in the UV-Vis spectra confirmed the increase in loading of the HSA-NPs with Pc4 or TT1 with the increasing amount of added photosensitizer (Figure S1). As it demonstrated in Figure S1, Pc4 gave a visible absorbance at 635 nm for concentrations >3.48  $\mu$ M Pc4 (Figure S1A), while TT1 already showed an absorbance signal at 1.58  $\mu$ M TT1 (Figure S1B). Fluorescence emission spectra confirmed the absorbance data as expected.



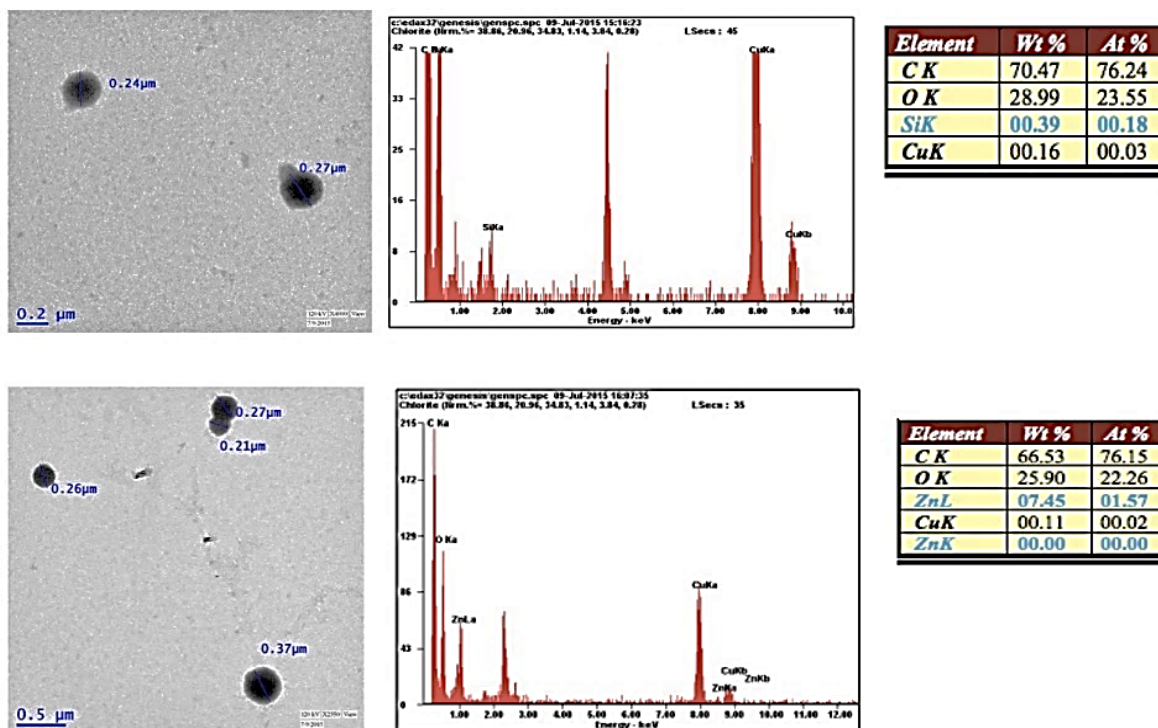


Figure 2. Representative transmission electron microscopy images (left) and energy-dispersive x-ray spectroscopy (EDS) (right) spectra of Pc4-HSA-NPs (Upper panel) and TT1-HSA-NPs (Lower panel) are depicted. The EDS spectra confirmed the presence of the Pc4 in the nanoparticles.

In order to confirm the localization of the photosensitizers within the NPs we performed TEM with energy-dispersive x-ray spectroscopy (EDS) analysis. TEM images in Figure 2 show spherical HSA-NPs for which the EDS analysis confirmed a Si signal of Pc4 in the area of the NPs (upper panel) and Zn indicative for TT1 loaded on the HSA-NPs (lower panel). TEM images show that the NPs with the highest content of Pc4 or TT1 give single well-defined spheres with a smooth surface and a diameter of 200–300 nm.

In addition to TEM, which shows the size of the dehydrated particles (Figure 2), the hydrodynamic diameter was determined by dynamic light scattering (Figure 3 and Tables S1–S4). In DLS, the hydrodynamic diameter for the TT1 loaded HSA-NPs was around 203 nm with a PDI of 0.15.

Next, we tested the stability of the dye-loaded HSA-NPs in different conditions (saline at 37°C 50% FBS at 37°C (condition in blood),

H<sub>2</sub>O at 4°C (storage condition)). In order to determine the dye leakage in serum conditions, which plays a crucial role in predicting the in vivo behavior, we incubated Pc-loaded HSA-NPs for 24 hours at 37°C in high-serum concentrations (50%) to mimic the conditions in the body (Figure 2B, D). The release profile of the Pc-loaded nanoparticles kept in water at 4°C for up to 6 weeks can be found in Tables S3 and S4.

At a temperature of 37 °C and in the presence of 50% (v/v) FBS, the release profile for TT1-HSA showed a burst release around 3% of TT1 and then no more release up to 8 hours. (The initial burst release may be due to the release of molecules loosely attached to the NP surface.) The slight increase in the hydrodynamic diameter indicates a swelling of the particles consistent with an entry of water molecules and a loosening of the NP matrix. After 8 hours a stronger leakage of TT1 was observed.

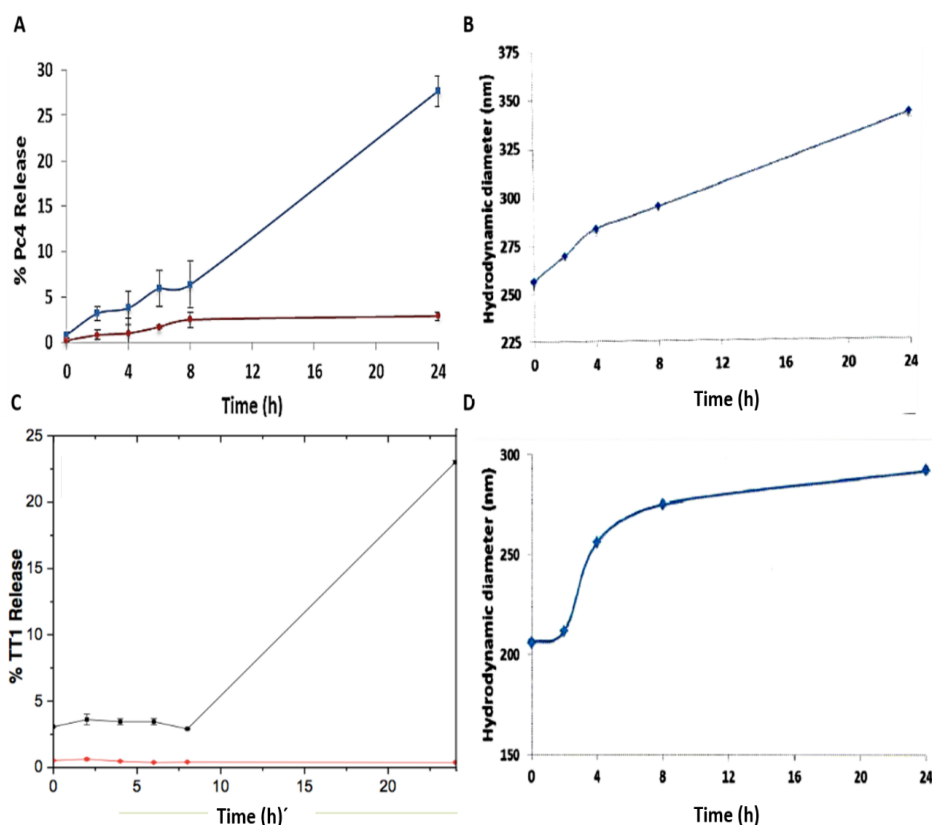


Figure 3. Time-dependent release of (A) Pc4 or (C) TT1 from HSA-NPs in 50% (v/v) fetal bovine serum (FBS) (blue line) or saline at 37°C (red line). Panels B and D show the change of the hydrodynamic diameter measured in 50% FBS at 37°C for human serum albumin nanoparticles loaded with Pc4 (B) and TT1 (D). The lines serve only to guide the eye.

Pc4-NP leaked continuously but slowly dye from the nanoparticles (Figure 3A). For both dyes, it was observed that after 24 hours the Pc release reached around 25% of the dye content. In contrast, the NPs loaded with Pc4 or TT1 stored in physiological saline solution (0.9% NaCl) showed negligible release of the dye, even after 24 hours at 37 °C.

The particles exhibited a satisfying shelf-life, (stability and Pc4 release in Milli-Q grade water at 4°C) the Pc4-loaded NP solutions showed no release of the Pc4 and no significant change in the PDI or hydrodynamic diameter for up to 4 weeks. The NPs (HSA-Pc4 and HSA-TT1) were found to be stable in pure water for 6 weeks at 4 °C, after which the NPs seem to break down (Table S1). The difference in the release profiles in FBS indicates that the Pc4 and the TT1 are bound in different ways to the scaffold of cross-linked HSA. This is also confirmed by the FTIR measurements (Figure 4). ATR-FTIR was performed to detect the effect of the phthalocyanine dyes within the

HSA structure and its conformation that play a role in the NP stability. HSA-NPs exhibited a significant shift in the protein amide I band arising from the C=O stretch from 1674 cm<sup>-1</sup> to 1659 cm<sup>-1</sup> with respect to HSA in solution, which can be explained by the glutaraldehyde-protein cross-linking during the NP formation. Further evidence of conformational changes of HSA in the HSA-NPs could be obtained from the shift in the stretching vibration of the N-H bond from 3301 cm<sup>-1</sup> to 3310 cm<sup>-1</sup>. The amide-II band at 1540 cm<sup>-1</sup> arising from the C-N stretching coupled with the N-H bending vibration was not shifted but showed a reduced intensity. FTIR results indicate structural changes arising from intramolecular bonding: a phenomenon probably arising from the conformational changes of the protein when it forms a nanoparticle from its native state. The presence of TT1 resulted in further red shift of the amide-I band to 1656 cm<sup>-1</sup> but left the amide-II band unchanged.

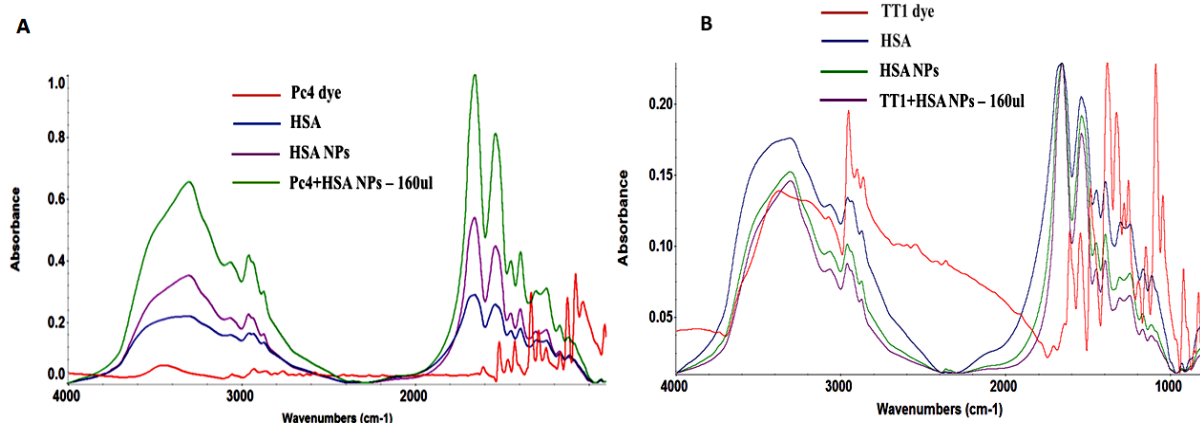


Figure 4. ATR-FTIR spectra of (A) Pc4 and (B) TT1-loaded human serum albumin (HSA) nanoparticles (NPs), empty HSA-NPs, human albumin solution, and the photosensitizer alone.

Both bands were of slightly reduced intensities in comparison to the unloaded HSA-NPs indicating the minor changes in the protein conformation arising from reorganized intra- and intermolecular bonding in presence of TT1

The presence of Pc4 exhibited pronounced changes in the intensities of both the amide-II bands but did not display any shift in the wave numbers for the respective Amide bands. Such enhanced alteration in the intensities were indicative of significant protein conformational changes that could have a role in the reorganization of protein secondary structures.

### Nanoparticle uptake and cytotoxicity

The toxicity of the HSA NP loaded with TT1 or Pc4 were tested by an MTS test on RAW264.7 macrophages as a model for off-target cells which can accumulate high quantities of the NPs by unspecific uptake.

Figure 4 displays the toxicity of photosensitizer loaded NPs tested at different concentrations (0–25 ng/ $\mu$ L for TT1 and 0–250 ng/ $\mu$ L for Pc4).

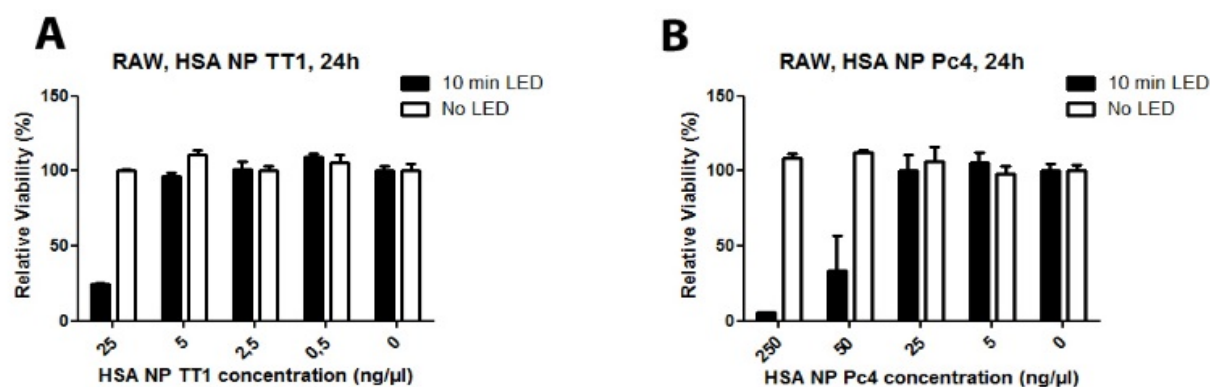


Figure 5. MTS test for cyto- (white bars) and photocytotoxicity induced by singlet oxygen production (black bars) of TT1-human serum albumin nanoparticles (HSA-NPs) (A) in the concentration range from 0.5 to 25 ng/ $\mu$ L and Pc4-hsa-NP (B) in the concentration range from 5 to 250 ng/ $\mu$ L on RAW264.7 macrophages after 24 hours of incubation. The treated cells were illuminated with a custom-made LED device for 10 minutes. Non-illuminated cells were used as a control.

MTS test on RAW264.7 macrophages indicated an extremely low toxicity of HSA-NPs even at higher concentrations (Figure 5, white bars). The ability of photosensitizer (Pc4, TT1) loaded HSA-NPs to trigger apoptosis by light-induced singlet oxygen production was

studied in macrophages, the intended target cells for the PDT treatment.

RAW264.7 cells were exposed to increasing concentration of the NPs and the IC<sub>50</sub> value was estimated (Figure 5). Cells then were illuminated with a custom-made LED device

for 10 minutes, with an energy of 3.04 mW/cm<sup>2</sup> (1824 mJ/cm<sup>2</sup>). Non-illuminated cells were used as control for the dark toxicity of the NPs. For HSA NP containing TT1, the value was 17.5 ng/μL (Figure 5A; black bars). HSA NP with Pc4 showed cell-killing efficacy with IC<sub>50</sub>-value of 45 ng/μL (Figure 5B; black bars). Next, we wanted to investigate the cellular uptake and localization of the loaded nanoparticles (Pc4-HSA-NPs and TT1-HSA-NPs). Therefore, we incubated RAW264.7 cells with 200 μg/μL NPs and visualized them by confocal microscopy at different time points up to 24 h (Figure 6 and S1). In Figure 6, the high

magnification merged confocal fluorescence microscopy and transmission image of the focal plane of some RAW cells incubated for 24 hours with 200 μg/mL TT1 HSA-NPs are shown. The image shows the cellular uptake and localization for TT1 HSA-NPs revealed by the first fluorescence signal inside the macrophages (RAW264.7 cells) after 2 hours of incubation. From the spotty appearance of the fluorescence signal (Figure 6, left) and the z stack in confocal microscopy (Figure 6 Right) at 24 hours incubation, we concluded that the nanoparticles are localized in vesicular structures such as endosomes.

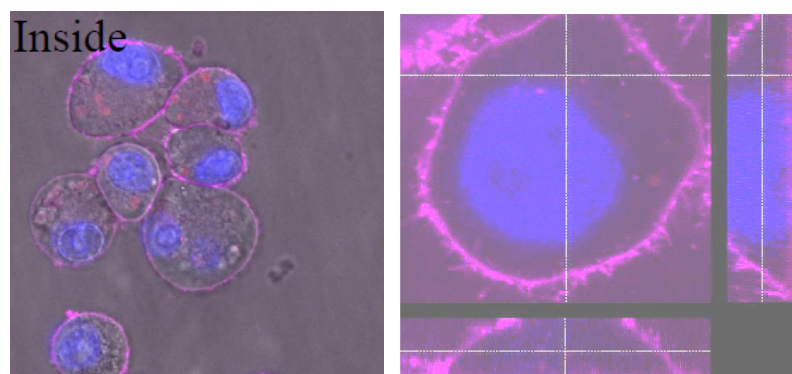


Figure 6. (left) high magnification merged confocal fluorescence microscopy and transmission image of the focal plane of RAW cells (right) z stack by confocal microscopy of a macrophage incubated for 24 hours with 200 μg/mL TT1 HSA nanoparticles. The blue fluorescence is due to Hoechts, a nuclear stain, the pink color indicates the red fluorescence of the membrane stain, CellMask. The red signal is due to the fluorescence signal of TT1. The micrograph confirms the morphological appearance of the macrophage.

Both the distribution of the NPs as well as the time before NP entry differed significantly between TT1 loaded and Pc4 loaded HSA-NPs (Figure S1). As it can be seen in Figure S1A, Pc4 homogeneously stained the cytoplasm of the cells even after 30 minutes of incubation while TT1 appears in defined spots indicative for endocytic uptake after 4 hours. In order to understand the unusual fast entry and cytosolic distribution of the Pc4, we tested the particles for the presence of free dye with a test developed in our lab.<sup>44</sup> We incubated red blood cells for less than 1 hour with the free Pc4 or TT1 dye at 100 ng/μL and 0.2 ng/μL and with the respective dye-loaded NPs at the same concentrations. While for TT1 no indication of free dye was evident, Pc4 NPs gave a strong signal (data not shown). Therefore, the internalization of the Pc4 from the HSA-NPs is indicative for free dye.<sup>44</sup> This is supported by our data in the stability of Pc4 loaded HSA-NPs

in presence of FBS at elevated temperature where a continuous release of dye from the NPs was detectable and the IR data that showed that the binding of TT1 to the HSA particles is different from that of Pc4 and the interaction of Pc4 with the HSA matrix of the NP is much weaker.

#### TT1-HSA-NPs administration in an atherosclerotic mouse model

The biodistribution of HSA NP loaded with TT1 was studied (Figure 3) in a mouse model of atherosclerosis in order to measure if the HSA accumulate preferentially in the plaques or other specific organs. At different time points (30 minutes, 3 hours, and 24 hours) after intravenous bolus injection of the 1mg/kg (=0.5 mg NP/mL) dose the mouse was sacrificed and selected organs (liver, lungs, spleen, kidneys) and atherosclerotic plaque in the carotid artery were screened for the fluorescence signal from TT1 (Figure 7 and S2 in SM).



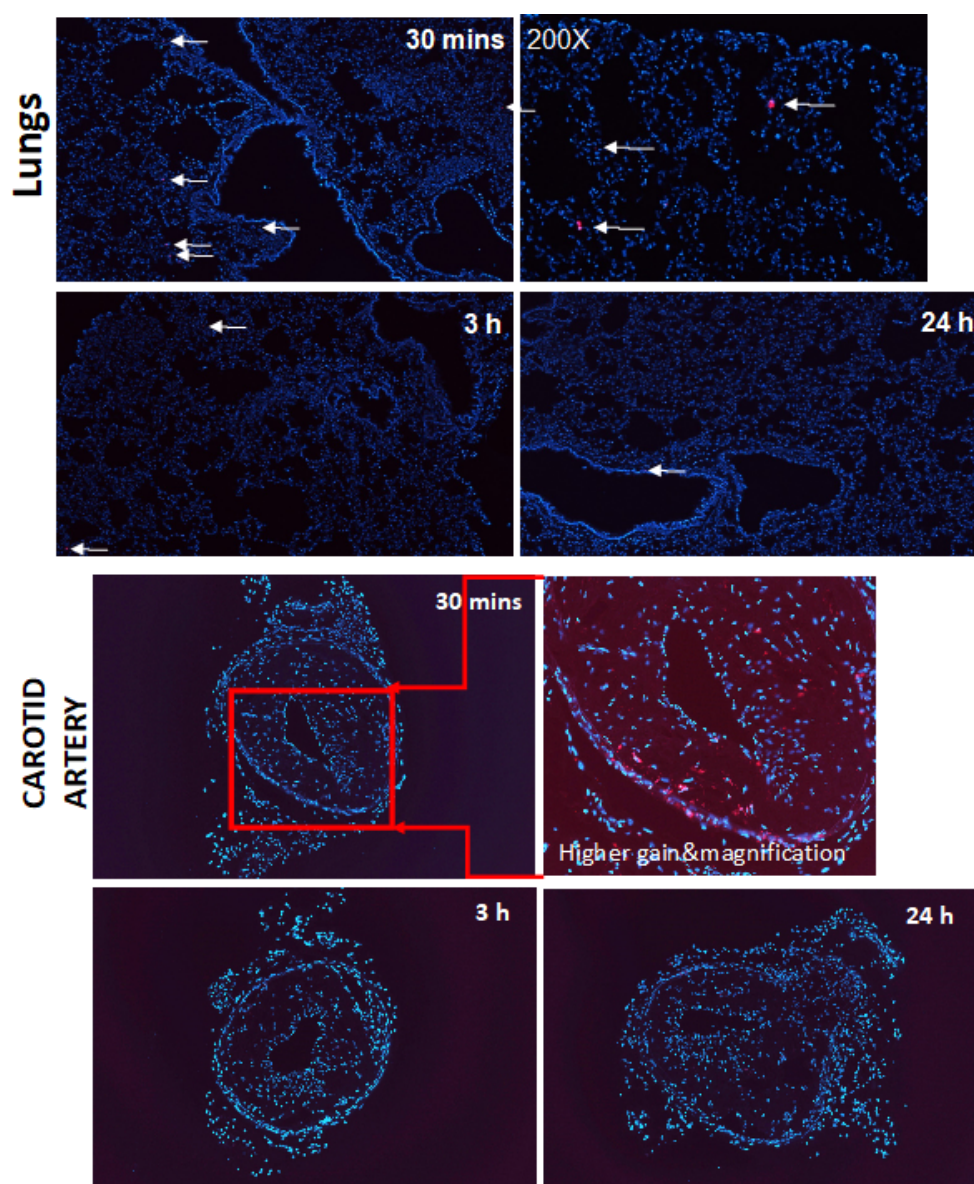


Figure 7. Upper panel: Fluorescence microscopy image from the lungs of a mouse injected with 1 mg/kg TT1-human serum albumin (HSA) nanoparticles (NPs) after 30 minutes, 2 hours, and 24 hours. Original magnification 100 $\times$ . Lower panel: Fluorescence microscopy image from the carotid artery of a mouse injected with 1 mg/kg TT1-HSA NP after 30 minutes, 2 hours, and 24 hours. Original magnification 100 $\times$ . In the micrograph taken at 30 minutes, the vessel wall is indicated by a white line while the lumen of the vessel is indicated by a pink line. The area between the 2 lines presents an atherosclerotic plaque obstructing the vessel. The magnification of the image at 30 minutes shows a low fluorescence signal of the TT1 observable only with maximum gain (inset).

Organs from untreated mice were imaged to determine the level of autofluorescence in the wavelength range relevant for TT1 detection. We focused mainly on organs known to accumulate nanoparticles. No fluorescence was observed at any of the measured timepoints in spleen, liver, and kidneys (Figure S2) as well as the organs from untreated mice (data not shown). In contrast, in the lungs (Figure 7 upper panel) and in the lesions in the carotid arteries

(Figure 7 lower panel) of nanoparticle-treated mice 30 minutes after treatment several fluorescent particles (arrows) could be detected. At later time points no fluorescence signal was detected in any of the tested organs except in the lungs. The observed low signal in the plaque as well as the disappearance of the fluorescence at later time points indicate a fast clearance of the HSA-NPs.

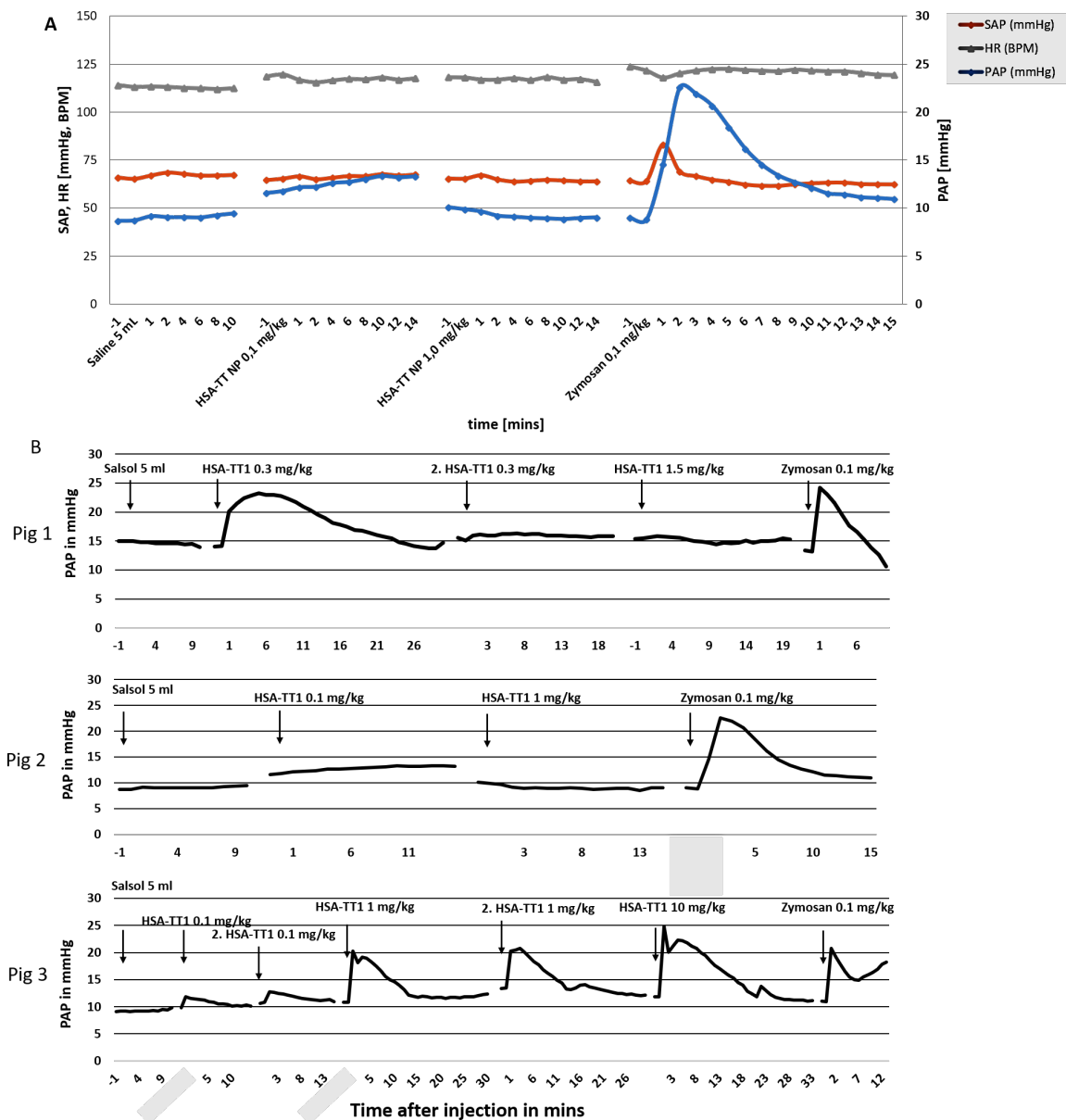


Figure 8. (A) Flow chart of the pulmonary arterial pressure (PAP), systemic arterial pressure, and HR after bolus injection of TT1-human serum albumin nanoparticles (HSA-NP) in pig 2 at different concentrations, saline as negative control and Zymosan as positive control. (B) Comparison of PAP in 3 pigs receiving different preparations of HSA-TT1 nanoparticles. Pig 1: male, 21 kg, each solution was prepared separately and shipped, max. conc: 1.25 mg NP/mL; Pig 2: male, 21 kg, each solution was prepared separately and shipped, max. concentration: 1.25 mg NP/mL; and Pig 3: male, 24 kg, stock solution 15 mg NP/mL prepared fresh from powder. The diagrams show the PAP in mmHg and the time after injection in mins while the arrows indicate the administration of each new drug.

### TT1-HSA-NPs administration in pigs

A problem frequently limiting the translation of nanodrugs in particular liposomal formulations into the clinics is a hypersensitivity reaction observed in sensitive patients, also named complement activation-related pseudoallergy (CARPA).<sup>53,54</sup> The symptoms, often a significant increase of PAP along with potential changes in HR indicate

cardiopulmonary distress. Cardiopulmonary distress caused by the nanoparticles can be critical for CVD patients. Therefore, we determined potential cardiopulmonary distress induced by the HSA-NPs in in vivo experiments in pigs.

Pigs present an animal model which can predict a pseudoallergic response in a fraction of human patients. TT1-HSA-NPs were tested

in concentrations ranging from 0.1 to 10 mg/kg per pig. PAP, SAP, and HR were monitored as sensitive parameters to determine a potential response to the NP injection (Figure 8A).

Mild to severe changes in the PAP of the pigs were observed in a concentration dependent manner (Except in pig 2). In pig 3, the TT1-HSA-NPs triggered severe PAP changes in a concentration dependent manner. The small but repeatable reaction indicated the absence of self-induced tolerance (tachyphylaxis). The 1.0 mg/kg evoked mild, >50% increase of PAP that remained in the physiological range. However, especially for the 1 mg NP/kg we observed the strongest dependence on the preparation conditions for the initial stock solution (Figure 8B comparison of pig 1–3). The 10× higher

dose evoked severe cardiovascular change with PAP elevation (Figure 8B pig 3), transient SAP decline and HR increase (data not shown). The induced change was the same increase in the PAP as the positive control zymosan (0.1 mg/kg) evoked reaction.

For the other two tested pigs that were injected with significantly lower concentration of NP solutions we observed only very mild reactions (Figure 8B pig 1) to the HSA NP suspensions if at all (Figure 8B pig 2). In order to understand the reason for the PAP increase we tested the plasma level of thromboxane (TxB2) and the activation of complement. For pig 3 which showed the strongest reaction a blood sample was analyzed for the TxB2 level (Figure 9).

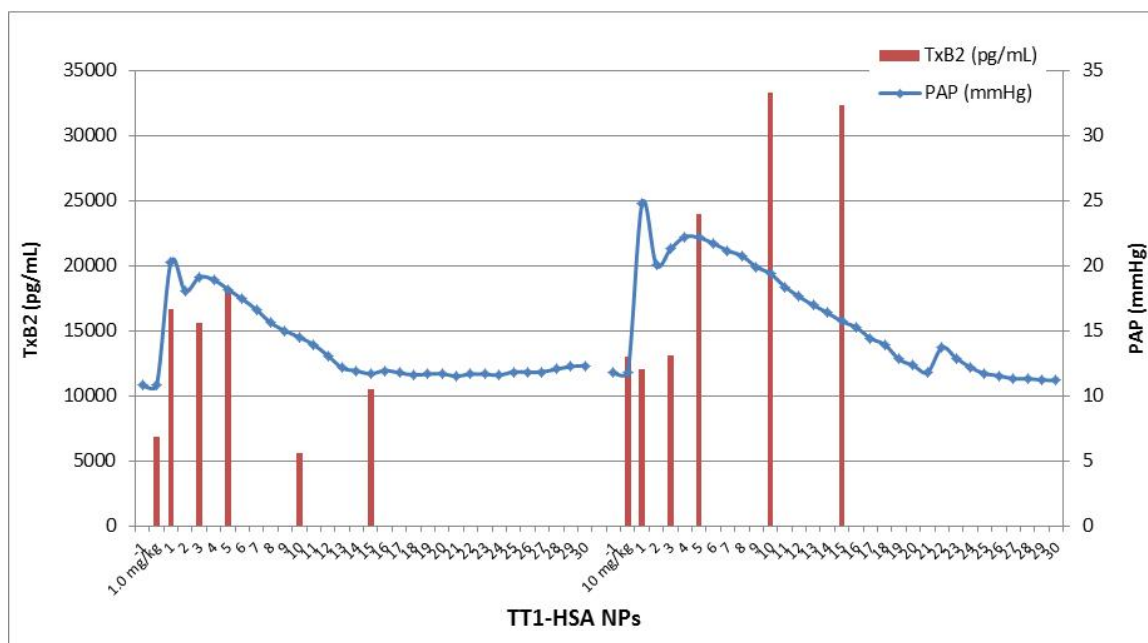


Figure 9. Pulmonary arterial pressure and plasma TxB2 levels for the TT1-human serum albumin doses of 1 and 10 mg/kg (stock nanoparticles concentration: 15 mg/mL) weight injected in pig 3.

PAP and plasma TxB2 increase after bolus injection of the TT1-HSA doses in pig 3. Together with the increase of PAP, a dose-dependent TxB2 elevation was observed (2.7 and 4.9-fold maximal elevation, respectively). However, for this high particle concentration, we observed an increasing turbidity of the solution which can indicate a flocculation that may be responsible for rapid PAP rises. The individual roles of complement activation, NP aggregation and direct activation of pulmonary

intravascular macrophages (PIM cells)<sup>48</sup> in the rapid PAP response to HSA NP injection need to be explored in the future. The precise mechanism for the contradicting immunoreactivity of the HSA-NPs or more general of nanomedicines is still under debate.<sup>55</sup>

After the observation of the adverse effect of the higher concentrated HSA-NPs solution we reanalyzed the solution by DLS and for the release of the TT1 (Table 1).

Table 1. Characterization of fresh TT1 HSA-NPs (15 mg/ml) and after 2 weeks of storage in physiologic saline at 4°C.

Sample Name	Size [nm]	PDI	% released dye
TT1-HSA-NPs (immediately after preparation)	290.6±8.5	0.261±0.094	n.d.
TT1-HSA-NPs (after 2 weeks storage)	671.4±36	0.695±0.068	2.65

HSA = human serum albumin; NP = nanoparticles; PDI = polydispersity index.

The reanalysis of the more concentrated nanoparticles by DLS confirmed our observation that the NP suspension is not stable at this high concentration. For the same NPs at a lower concentration of 1 mg/mL NP suspension, we observed at 4°C in water no change for up to 4 weeks.

#### In vitro complement activation

A significant aspect in the use of nanoparticles as a drug delivery system is additionally to their low toxicity in general their

interaction with the immune system. In order to determine if TT1 loaded HSA-NPs activate complement, they were added to 3 serum samples of human blood donors and their potential to increase C5a and sC5b-9 levels were measured (Figure 10). It is important to note that the experiments were carried out with separate serum samples and not with pooled blood.

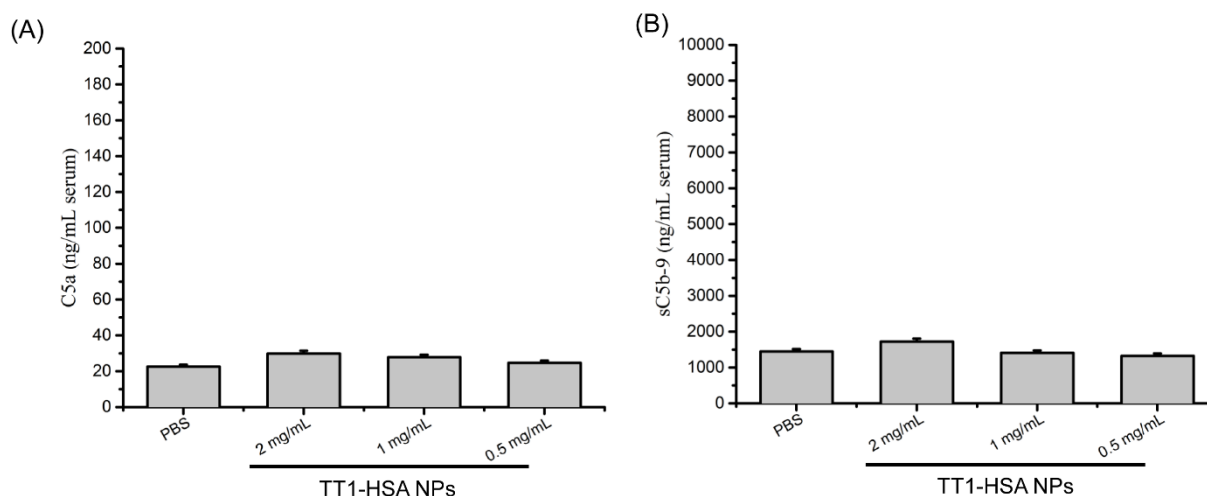


Figure 10. Effect of TT1-human serum albumin nanoparticles on human complement in vitro. Complement activation markers (A) C5a, (B) sC5b-9. Blank (phosphate buffer solution) and positive control (1 mg/mL Zymosan) were tested for one serum was shown. Zymosan-induced rises of serum C5a and sC5b-9 levels were 170 ng/mL serum and 36722 ng/mL serum (not shown), respectively. Each experiment was repeated with 3 individual sera. Activation pattern was similar in other tested sera.

Results show that TT1-HSA-NPs up to 2 mg/mL concentration are poor activators of the terminal pathway of the human complement system. Since Hamblin (one of the pioneers in the field of PDT of macrophage targeting Pc) suggested its use for vulnerable plaques in cardiovascular disease<sup>56,57</sup> and the first patent in

199423, research aiming to localize, image, and treat vulnerable plaques in a non- or minimally invasive way was intensified. The factors defining plaques as vulnerable to rupture have high macrophage infiltration, a thin fibrotic cap and extended necrotic core.<sup>58,59</sup> The review of Hellings et al.<sup>59</sup> summarizes that the main



problem of a contrast agent free detection is a limitation of the sensitivity and/or specificity as only the calcification (i.e., stable plaques) can be detected with 100% in computed tomography and hemorrhage (ruptured plaque) in MRI. The most promising technique is optical coherence tomography with satisfying confidence in both sensitivity and specificity and a high spatial resolution, which is important for early detection of plaques and macrophages. However, these techniques allow only visualization without the possibility of treatment. Hence, simultaneous detection and treatment of vulnerable plaques and especially the infiltrating macrophages is a still unmet medical need.

In the present study, we described the biological profile of glutaraldehyde cross-linked albumin NPs loaded with the novel NIR photosensitizer, TT1. These NPs were tested for light-induced toxicity in macrophages as attempted target cells for CVD PDT, immunoreactivity measured *in vitro* by complement activation and *in vivo* by cardiovascular distress syndrome in pigs as well as their accumulation in arteriosclerotic plaque *in vivo* in a mouse model.

Several other works reported about the use of Pc for the treatment as a cancer drug or as a treatment for arteriosclerosis. Davanzo et al.<sup>60</sup> published a study in which they investigate the role of the light source and dose on the efficiency of AIPc delivered by albumin NPs to induce cell death in glioma cells *in vitro*. A direct comparison with our results is difficult as the highest light dose used by them with the LED is significantly lower than in our experiments and the loading efficacy of the photosensitizer to the albumin NPs is missing. However, they found that the most efficient light source is the continuous wave laser illumination at low non-toxic light doses. In our case even at the high light dose, which is 2.6-times higher, we did not observe any phototoxicity on the cells without the photosensitizer. Even the targeted delivery of albumin-conjugated Pc to tumor-infiltrating macrophages was reported in previous studies.<sup>61</sup> Brasseur et al.<sup>61</sup> reported the selective uptake of AIPc covalently bound to maleylated bovine serum albumin BSA molecules by tumor-infiltrating macrophages in comparison to non-macrophage cell lines. They

required the conjugation of the Pc molecules because in order to have an increased uptake and a shift from membrane damage induced necrosis to apoptosis.

The fluorescence images of the RAW cells treated with our NPs showed a high amount of photosensitizer located within the cell that will induce a preferential intracellular cell damage leading to apoptosis even without a targeting molecule. Our observation that the albumin NPs without light activation are well-tolerated by the cells is in good agreement with the non-toxicity of the BSA conjugates found by Brasseur and co-workers.<sup>61</sup> In a recently published work Molina et al.<sup>62</sup> compared the delivery of glutaraldehyde cross-linked HSA-NPs for the delivery of photosensitizer Ce6 to tumor cells with NPs cross-linked with a redox-sensitive cross-linker, which will break down in presence of glutathione in the cell cytosol. Here, differently from our approach, the photosensitizer was covalently bound to the albumin NPs. In summary, they observed a much lower cell-killing efficacy of glutaraldehyde cross-linked NPs that are not releasing the dye as compared to the redox-sensitive NPs.<sup>62</sup> This is in good agreement with our observation that the quantum yield of the NP bound dye is usually lower than that of the free Pc in DMSO. One possible explanation is that the produced singlet oxygen is partially degrading the albumin matrix rather than being released.

The stark contrast between our results in human serum, where no complement activation took place, and the pig experiments, which showed a significant increase in thromboxane and a hyperreaction in terms of increase in pulmonary arterial pressure needs an explanation.

The fast accumulation of the lungs we observed in the mice can explain the contradictory results about the absence of complement activation in human serum and the hyperreactivity of the pigs. Earlier experiments with albumin microparticles in pigs showed that hyperreactivity in pigs can be due to the accumulation of the material in PIMs and may cause a significant increase in plasma TxB2 levels<sup>63,64</sup> which is in accordance to our own observations. The studies reported also that the immune response is strongly species-dependent and is rarely observed in humans.

## Summary

Summarizing the results, we have found that TT1 loaded HSA-NPs localize in the endosomal vesicles rather than in the cell membrane, and when illuminate they show a good cell-killing activity in the low  $\mu\text{g/mL}$  range with low immunoreactivity in vivo and complement activation potential in vitro. In an atherosclerotic mouse model, loaded nanoparticles localized in the plaques 30 minutes after injection in the tail vein. The localization of TT1-loaded NPs in the plaques allows the visualization of atherosclerotic areas in vessels and offers high-singlet oxygen production along with NIR light-induced macrophage killing, fulfilling some of the requirements for a candidate as a contrast agent and PDT treatment for CVD.

## Funding:

The research leading to these results has received funding from FP7-NMP CosmoPHOS-Nano under grant agreement No. 310337. Additional funding was received by the Spanish groups from MINECO (CTQ2017-85393-P) and ERA-NET/MINECO EuroNanoMed2017-191 / PCIN-2017-042.

## Bibliography

1. [https://www.who.int/news-room/fact-sheets/detail/cardiovascular-diseases-\(cvds\)](https://www.who.int/news-room/fact-sheets/detail/cardiovascular-diseases-(cvds))
2. Heidenreich, P. A.; Trogon, J. G.; Khavjou, O. A.; Butler, J.; Dracup, K.; Ezekowitz, M. D.; Finkelstein, E. A.; Hong, Y.; Johnston, S. C.; Khera, A.; et al. Forecasting the Future of Cardiovascular Disease in the United States: A Policy Statement From the American Heart Association. *Circulation* 2011, 123 (8), 933–944.
3. Libby, P.; Ridker, P. M.; Maseri, A. Inflammation and Atherosclerosis. *Circulation* 2002, 105 (9), 1135–1143.
4. Libby, P.; Ridker, P. M.; Hansson, G. K. Progress and Challenges in Translating the Biology of Atherosclerosis. *Nature* 2011, 473 (7347), 317–325.
5. Naghavi, M.; Libby, P.; Falk, E.; Casscells, S.; Litovsky, S.; Rumberger, J.; Badimon, J.; Stefanadis, C.; Moreno, P.; Pasterkamp, G.; et al. From Vulnerable Plaque to Vulnerable Patient a Call for New Definitions and Risk Assessment Strategies: Part I. *Circulation* 2003, 108 (14), 1664–1672.
6. Ibanez, B.; Vilahur, G.; Badimon, J. J. Plaque Progression and Regression in Atherothrombosis. *J. Thromb. Haemost.* 2007, 5 (s1), 292–299.
7. Mallika, V.; Goswami, B.; Rajappa, M. Atherosclerosis Pathophysiology and the Role of Novel Risk Factors: A Clinicobiochemical Perspective. *Angiology* 2007, 58 (5), 513–522.
8. Sary, H. C. Natural History and Histological Classification of Atherosclerotic Lesions an Update. *Arterioscler. Thromb. Vasc. Biol.* 2000, 20 (5), 1177–1178.
9. Tabas, I.; García-Cardena, G.; Owens, G. K. Recent Insights into the Cellular Biology of Atherosclerosis. *J. Cell Biol.* 2015, 209 (1), 13–22.
10. MacNeill, B. D.; Jang, I. K.; Bouma, B. E.; Iftimia, N.; Takano, M.; Yabushita, H., ... & Tearney, G. J. Focal and Multi-Focal Plaque Macrophage Distributions in Patients with Acute and Stable Presentations of Coronary Artery Disease. *J. Am. Coll. Cardiol.* 2004, 44 (5), 972–979.
11. Janssen, M. Electrosurgical Catheter and Method for Resolving Atherosclerotic Plaque by Radio Frequency Sparking. Google Patents October 3, 1995, p US5454809.
12. Rockson S. G., Lorenz D. P., Cheong W. F., Woodburn K. W. Photoangioplasty: An emerging clinical cardiovascular role for photodynamic therapy. *Circulation.* 2000, 102(5), 591-6.
13. Da Collina, G. A.; Tempestini-Horliana, A. C. R.; da Silva, D. de F. T.; Longo, P. L.; Makabe, M. L. F.; Pavani, C. Oral Hygiene in Intensive Care Unit Patients with Photodynamic Therapy: Study Protocol for Randomised Controlled Trial. *Trials* 2017, 18 (1), 385.
14. Prażmo, E.; Mielczarek, A.; Kwaśny, M.; Łapiński, M. Photodynamic Therapy As a Promising Method Used in the Treatment of Oral Diseases. *Adv. Clin. Exp. Med.* 2016, 25 (4), 799–807.
15. Soergel, P.; Löning, M.; Staboulidou, I.; Schippert, C.; Hillemanns, P. Photodynamic Diagnosis and Therapy in Gynecology. *J. Environ. Pathol. Toxicol. Oncol.* 2008, 27 (4), 307–320.

16. Luo, S.; Zhang, E.; Su, Y.; Cheng, T.; Shi, C. A Review of NIR Dyes in Cancer Targeting and Imaging. *Biomaterials* 2011, 32 (29), 7127–7138.
17. Dougherty, T. J.; Gomer, C. J.; Henderson, B. W.; Jori, G.; Kessel, D.; Korbelik, M.; Moan, J.; Peng, Q. Photodynamic Therapy. *JNCI J. Natl. Cancer Inst.* 1998, 90 (12), 889–905.
18. Wennink, J. W. H.; Liu, Y.; Mäkinen, P. I.; Setaro, F.; de la Escosura, A.; Bourajaj, M.; Lappalainen, J. P.; Holappa, L. P.; van den Dikkenberg, J. B.; al Fartousi, M.; et al. Macrophage Selective Photodynamic Therapy by Meta-Tetra(Hydroxyphenyl)Chlorin Loaded Polymeric Micelles: A Possible Treatment for Cardiovascular Diseases. *Eur. J. Pharm. Sci.* 2017, 107, 112–125.
19. Wu, L.-P.; Ficker, M.; Mejlsoe, S. L.; Hall, A.; Paolucci, V.; Christensen, J. B.; Trohopoulos, P. N.; Moghimi, S. M. Poly-(Amidoamine) Dendrimers with a Precisely Core Positioned Sulforhodamine B Molecule for Comparative Biological Tracing and Profiling. *J. Control. Release* 2017, 246, 88–97.
20. Wu, L.-P.; Ficker, M.; Christensen, J. B.; Trohopoulos, P. N.; Moghimi, S. M. Dendrimers in Medicine: Therapeutic Concepts and Pharmaceutical Challenges. *Bioconjug. Chem.* 2015, 26 (7), 1198–1211.
21. Spyropoulos-Antonakakis, N.; Sarantopoulou, E.; Trohopoulos, P. N.; Stefi, A. L.; Kollia, Z.; Gavriil, V. E.; Bourkoula, A.; Petrou, P. S.; Kakabakos, S.; Semashko, V. V.; et al. Selective Aggregation of PAMAM Dendrimer Nanocarriers and PAMAM/ZnPc Nanodrugs on Human Atheromatous Carotid Tissues: A Photodynamic Therapy for Atherosclerosis. *Nanoscale Res. Lett.* 2015, 10, 210.
22. Tang, G.; Hyman, S.; Schneider Jr, J. H.; Giannotta, S. L. Application of Photodynamic Therapy to the Treatment of Atherosclerotic Plaques. *Neurosurgery* 1993, 32 (3), 438–443.
23. Narciso, H. L. Method for Treating Cardiovascular Disease through Adjunctive Photodynamic Therapy. Google Patents March 29, 1994, p US5298018.
24. Yuan, A.; Wu, J.; Tang, X.; Zhao, L.; Xu, F.; Hu, Y. Application of Near-infrared Dyes for Tumor Imaging, Photothermal, and Photodynamic Therapies. *J. Pharm. Sci.* 2013, 102 (1), 6–28.
25. Huang, Z. A Review of Progress in Clinical Photodynamic Therapy. *Technol. Cancer Res. Treat.* 2005, 4 (3), 283–293.
26. Taquet, J. P.; Frochot, C.; Manneville, V.; Barberi-Heyob, M. Phthalocyanines Covalently Bound to Biomolecules for a Targeted Photodynamic Therapy. *Curr. Med. Chem.* 2007, 14 (15), 1673–1687.
27. Tedesco, A. C.; Rotta, J. C.; Lunardi, C. N. Synthesis, Photophysical and Photochemical Aspects of Phthalocyanines for Photodynamic Therapy. *Curr. Org. Chem.* 2003, 7 (2), 187–196.
28. Ogura, S. I.; Tabata, K.; Fukushima, K.; Kamachi, T.; Okura, I. Development of Phthalocyanines for Photodynamic Therapy. *J. Porphyr. Phthalocyanines* 2006, 10 (09), 1116–1124.
29. Master, A.; Livingston, M.; Gupta, A. S. Photodynamic Nanomedicine in the Treatment of Solid Tumors: Perspectives and Challenges. *J. Control. Release* 2013, 168 (1), 88–102.
30. Soler, D. C.; Ohtola, J.; Sugiyama, H.; Rodriguez, M. E.; Han, L.; Oleinick, N. L.; Lam, M.; Baron, E. D.; Cooper, K. D.; McCormick, T. S. Activated T Cells Exhibit Increased Uptake of Silicon Phthalocyanine Pc 4 and Increased Susceptibility to Pc 4-Photodynamic Therapy-Mediated Cell Death. *Photochem. Photobiol. Sci.* 2016, 15 (6), 822–831.
31. Ragoussi, M.-E.; Torres, T. Modern Synthetic Tools toward the Preparation of Sophisticated Phthalocyanine-Based Photoactive Systems. *Chem. Asian J.* 2014, 9 (10), 2676–2707.
32. Claessens, C. G.; Hahn, U.; Torres, T. Phthalocyanines: From Outstanding Electronic Properties to Emerging Applications. *Chem. Rec.* 2008, 8 (2), 75–97.
33. Baron, E. D.; Malbasa, C. L.; Santo-Domingo, D.; Fu, P.; Miller, J. D.; Hanneman, K. K.; Hsia, A. H.; Oleinick, N. L.; Colussi, V. C.; Cooper, K. D. Silicon Phthalocyanine (Pc 4) Photodynamic Therapy Is a Safe Modality for Cutaneous Neoplasms: Results of a Phase 1 Clinical Trial. *Lasers Surg. Med.* 2010, 42 (10), 728–735.

34. Chatterjee, D. K.; Fong, L. S.; Zhang, Y. Nanoparticles in Photodynamic Therapy: An Emerging Paradigm. *Adv. Drug Deliv. Rev.* 2008, 60 (15), 1627–1637.
35. Jia, X.; Jia, L. Nanoparticles Improve Biological Functions of Phthalocyanine Photosensitizers Used for Photodynamic Therapy. *Curr. Drug Metab.* 2012, 13 (8), 1119–1122.
36. Wennink J.W.H, Liu Y., Mäkinen P. I., Setaro F., de la Escosura A., Bourajaj M., Lappalainen J. P., Holappa L. P., van den Dikkenberg J.B., Al Fartousi M., Trohopoulos P. N., Ylä-Herttuala S., Torres T., Hennink W.E., van Nostrum C.F. Macrophage selective photodynamic therapy by meta-tetra(hydroxyphenyl)chlorin loaded polymeric micelles: A possible treatment for cardiovascular diseases. *Eur J Pharm Sci.* 2017, 107, 112-125. doi: 10.1016/j.ejps.2017.06.038. Epub 2017 Jul 2.
37. Spyropoulos-Antonakakis N1, Sarantopoulou E1, Trohopoulos PN2, Stefi AL1, Kollia Z1, Gavriil VE1, Bourkoula A3, Petrou PS3, Kakabakos S3, Semashko VV4, Nizamutdinov AS4, Cefalas AC5. Selective aggregation of PAMAM dendrimer nanocarriers and PAMAM/ZnPc nanodrugs on human atheromatous carotid tissues: a photodynamic therapy for atherosclerosis. *Nanoscale Res Lett.* 2015 May 7;10:210. doi: 10.1186/s11671-015-0904-5. ECollection 2015.
38. He H., Yuan Q., Bie J., Wallace R.L., Yannie P.J., Wang J., Lancina MG 3rd., Zolotarskaya O.Y., Korzun W., Yang H., Ghosh S. Development of mannose functionalized dendrimeric nanoparticles for targeted delivery to macrophages: use of this platform to modulate atherosclerosis. *Transl Res.* 2018, 193, 13-30. doi: 10.1016/j.trsl.2017.10.008.
39. Cid, J.-J.; Yum, J.-H.; Jang, S.-R.; Nazeeruddin, M. K.; Martinez-Ferrero, E.; Palomares, E.; Ko, J.; Graetzel, M.; Torres, T. Molecular Cosensitization for Efficient Panchromatic Dye-Sensitized Solar Cells. *Angew. Chemie Int. Ed.* 2007, 46 (44), 8358–8362.
40. Enes, R. F.; Cid, J.-J.; Hausmann, A.; Trukhina, O.; Gouloumis, A.; Vazquez, P.; Cavaleiro, J. A. S.; Tome, A. C.; Guldi, D. M.; Torres, T. Synthesis and Photophysical Properties of Fullerene-Phthalocyanine-Porphyrin Triads and Pentads. *Chem. - A Eur. J.* 2012, 18 (6), 1727–1736.
41. Oleinick, N.; Antunez, A.; Clay, M.; Rihter, B.; Kenney, M. New Phthalocyanine Photosensitizers for Photodynamic Therapy. *Photochem. Photobiol.* 1993, 57 (2), 242–247.
42. Li, Y. S.; Kenney, M. E. Methods of Syntheses of Phthalocyanine Compounds. Google Patents 1998, p US5763602.
43. Langer, K.; Balthasar, S.; Vogel, V.; Dinauer, N.; von Briesen, H.; Schubert, D. Optimization of the Preparation Process for Human Serum Albumin (HSA) Nanoparticles. *Int. J. Pharm.* 2003, 257 (1–2), 169–180.
44. Mukherjee, S.; Ray, S.; Thakur, R. Solid Lipid Nanoparticles: A Modern Formulation Approach in Drug Delivery System. *Indian J. Pharm. Sci.* 2009, 71 (4), 349.
45. Banerjee, S.; Pal, T. K.; Guha, S. K. Probing Molecular Interactions of Poly(Styrene-Co-Maleic Acid) with Lipid Matrix Models to Interpret the Therapeutic Potential of the Co-Polymer. *Biochim. Biophys. Acta - Biomembr.* 2012, 1818 (3), 537–550.
46. Wöhrle, D.; Shopova, M.; Müller, S.; Milev, A. D.; Mantareva, V. N.; Krastev, K. K. Liposome-Delivered Zn(II)-2,3-Naphthalocyanines as Potential Sensitizers for PDT: Synthesis, Photochemical, Pharmacokinetic and Phototherapeutic Studies. *J. Photochem. Photobiol. B Biol.* 1993, 21 (2–3), 155–165.
47. Kuznetsova, N.; Makarova, E.; Dashkevich, S.; Gretsova, N.; Kalmykova, E.; Negrimovsky, V.; Kaliya, O. L.; Lukyanets, E. A. Structure-Photochemical Properties Relationship for Porphyrins and Related Compounds. *Zh. Obs. Khim.* 2000, 70, 140–148.
48. Androzzzi, P.; Martinelli, C.; Carney, R. P.; Carney, T. M.; Stellacci, F. Erythrocyte Incubation as a Method for Free-Dye Presence Determination in Fluorescently Labeled Nanoparticles. *Mol. Pharm.* 2013, 10 (3), 875–882.
49. Andersen, A. J.; Robinson, J. T.; Dai, H.; Hunter, A. C.; Andresen, T. L.; Moghimi, S. M. Single-Walled Carbon Nanotube Surface Control of Complement Recognition and Activation. *ACS Nano* 2013, 7 (2), 1108–1119.
50. Banda, N. K.; Mehta, G.; Chao, Y.; Wang, G.; Inturi, S.; Fossati-Jimack, L.; Botto, M.; Wu, L.; Moghimi, S. M.; Simberg, D. Mechanisms of Complement Activation by Dextran-Coated



Superparamagnetic Iron Oxide (SPIO) Nanoworms in Mouse versus Human Serum. Part. Fibre Toxicol. 2014, 11 (1), 64.

51. Szebeni, J.; Baranyi, L.; Savay, S.; Bodo, M.; Morse, D. S.; Basta, M.; Stahl, G. L.; Bünger, R.; Alving, C. R. Liposome-Induced Pulmonary Hypertension: Properties and Mechanism of a Complement-Mediated Pseudoallergic Reaction. *Am. J. Physiol. Heart Circ. Physiol.* 2000, 279 (3), H1319-28.
52. Mészáros, T.; Kozma, G.; Shimizu, T.; Miyahara, K.; Turjeman, K.; Ishida, T.; Barenholz, Y.; Urbanics, R.; Szebeni, J. Involvement of Complement Activation in the Pulmonary Vasoactivity of Polystyrene Nanoparticles in Pigs: Unique Surface Properties Underlying Alternative Pathway Activation and Instant Opsonization. *Int. J. Nanomedicine* 2018, Volume 13, 6345–6357.
53. Urbanics, R.; Bedőcs, P.; Szebeni, J. Lessons Learned from the Porcine CARPA Model: Constant and Variable Responses to Different Nanomedicines and Administration Protocols. *Eur. J. Nanomedicine* 2015, 7 (3), 219–231.
54. Szebeni, J.; Bedőcs, P.; Csukás, D.; Rosivall, L.; Bünger, R.; Urbanics, R. A Porcine Model of Complement-Mediated Infusion Reactions to Drug Carrier Nanosystems and Other Medicines. *Adv. Drug Deliv. Rev.* 2012, 64 (15), 1706–1716.
55. Szebeni, J.; Simberg, D.; González-Fernández, Á.; Barenholz, Y.; Dobrovolskaia, M. A. Roadmap and Strategy for Overcoming Infusion Reactions to Nanomedicines. *Nat. Nanotechnol.* 2018. 13(12), 1100-1108. doi: 10.1038/s41565-018-0273-1
56. Liu, Q.; Hamblin, M. R. Macrophage-Targeted Photodynamic therapy: Scavenger receptor expression and activation state. *Int J Immunopathol Pharmacol.* 2005, 18 (3), 391–402.
57. Hamblin, M. R.; Miller, J. L.; Ortel, B. Scavenger-Receptor Targeted Photodynamic Therapy. *Photochem. Photobiol.* 2000, 72 (4), 533–540.
58. Virmani, R.; Burke, A. P.; Willerson, J. T.; Farb, A.; Narula, J.; Kolodgie, F. D. The Pathology of Vulnerable Plaque. *Vulnerable Atheroscler. Plaque Strateg. Diagnosis Manag.* 2007, 47 (8), 19–36.
59. Hellings, W. E.; Peeters, W.; Moll, F. L.; Pasterkamp, G. From Vulnerable Plaque to Vulnerable Patient: The Search for Biomarkers of Plaque Destabilization. *Trends Cardiovasc. Med.* 2007, 17 (5), 162–171.
60. Davanzo, N. N.; Pellosi, D. S.; Franchi, L. P.; Tedesco, A. C. Light Source Is Critical to Induce Glioblastoma Cell Death by Photodynamic Therapy Using Chloro-Aluminiumphthalocyanine Albumin-Based Nanoparticles. *Photodiagnosis Photodyn. Ther.* 2017, 19, 181–183.
61. Brasseur, N.; Langlois, R.; Madeleine, C. La; Ouellet, R.; Lier, J. E. Receptor-Mediated Targeting of Phthalocyanines to Macrophages Via Covalent Coupling to Native or Maleylated Bovine Serum Albumin. *Photochem. Photobiol.* 2008, 69 (3), 345–352.
62. Moraima Morales, A. M. M. Redox-Sensitive Cross-Linking Enhances Albumin Nanoparticle Function as Delivery System for Photodynamic Cancer Therapy. *J. Nanomed. Nanotechnol.* 2015, 06 (03), 1–20.
63. ØISTENSEN, J.; HEDE, R.; MYRENG, Y.; EGE, T.; HOLTZ, E. Intravenous Injection of Alburnex R Microspheres Causes Thromboxane Mediated Pulmonary Hypertension in Pigs, but Not in Monkeys or Rabbits. *Acta Physiol. Scand.* 1992, 144 (3), 307–315.
64. Walday, P.; Tolleshaug, H.; Gjøen, T.; Kindberg, G. M.; Berg, T.; Skotland, T.; Holtz, E. Biodistributions of Air-Filled Albumin Microspheres in Rats and Pigs. *Biochem. J.* 1994, 299 (2), 437–443.
65. J. Ma, J.Y. Chen, M. Idowu, T. Nyokong, Generation of Singlet Oxygen via the Composites of Water-Soluble Thiol-Capped CdTeQuantum Dots-Sulfonated Aluminum Phthalocyanines. *J. Phys. Chem. B*, 2008, 112, 15.

Quote as: Banerjee S, Sengupta J, Aljarilla A, Setaro F, Mäkinen PI, Wu LP, Holappa L, Escosura A, Martinelli C, Trohopoulos PN, Ylä-Herttuala S, Urbanics R, Szebeni J, Torres T, and Krol, S, Human serum albumin nanoparticles loaded with the NIR phthalocyanine dyes for potential use in photodynamic therapy of atherosclerotic plaques, *Prec. Nanomed.* 2019 Apr;2(2):278-302, [https://doi.org/10.33218/prnano2\(2\).190411.1](https://doi.org/10.33218/prnano2(2).190411.1)

## Supplementary information

Table S1. Influence of solvent and experimental conditions at fast addition on the size of HSA nanoparticles

Solvent 1	Solvent 2	ratio	Volume [ml]	Hydrodynamic diameter	PDI (one peak)
Ethanol	-		2	249.9± 13.61	0.263± 0.051
Ethanol	Water	7:1	2	289.5 ±7.2	0.219± 0.09
Ethanol	Methanol	2.4:5.6	2	269.2 ±4.25	0.339± 0.015
Acetone	-		1) 1	316.5± 5.15	0.18± 0.031
			2) 2	218.4± 8.12	0.375± 0.045
Acetone	Water	7:1	1) 1	278.6 ±36.24	0.508± 0.166
			2) 2	172.9± 6.14	0.498± 0.087
Acetone	Water	6:2	2	127.6± 3.39	0.165± 0.019

Table S2. HSA nanoparticle parameters versus photosensitizer concentration for Pc4-HSA and TT1-HSA NPs

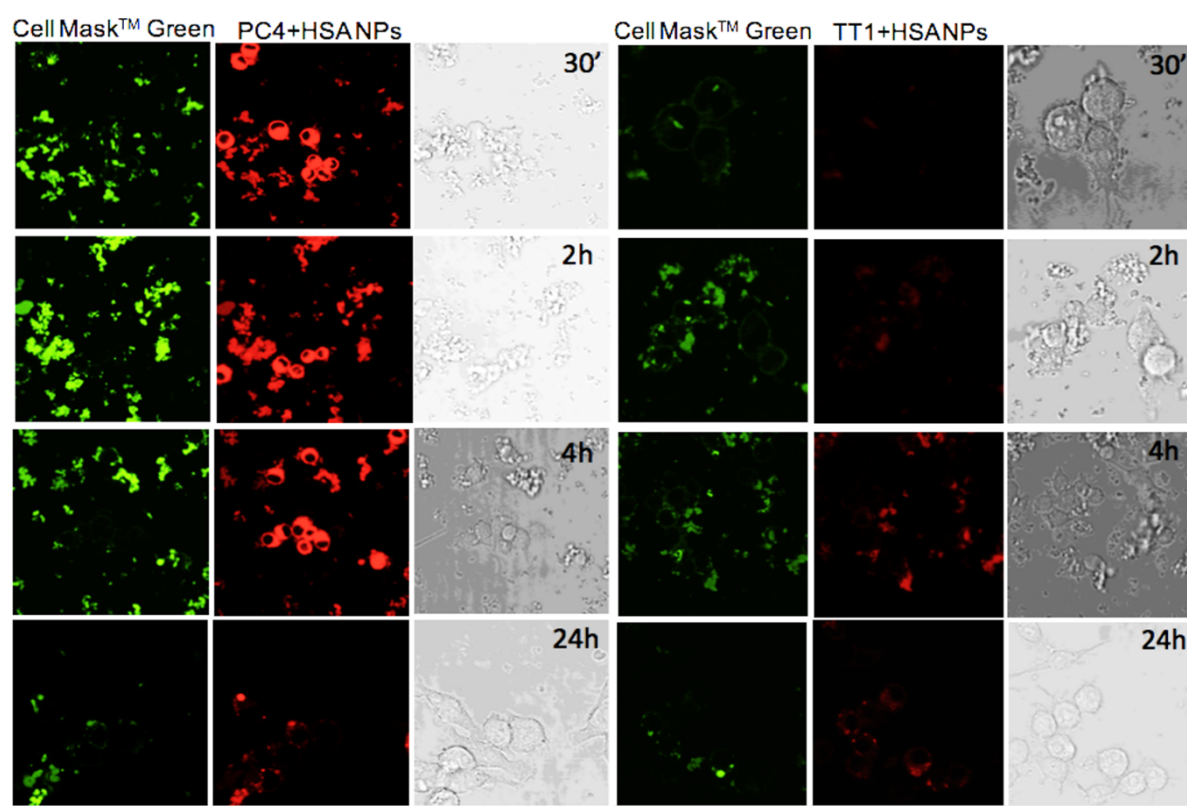
Sample	Added Dye Conc [mM]	Diameter [nm]	PDI	Zeta potential [mV]	Encapsulation efficiency [%]	Singlet O <sub>2</sub> Quantum
Pc4-HSA	0.70	248.3± 5.3	0.2±0.02	-13.3±0.5	47.7	0.0142
Pc4-HSA	1.04	266.4± 1.2	0.21±0.05	-22.5±1.3	60.2	0.063
Pc4-HSA	1.40	284.4± 1.4	0.27±0.04	-25.7±0.5	69.2	0.099
TT1-HSA	0.63	203.6± 7.1	0.15±0.06	-28.8±0.1	40.5	0.016
TT1-HSA	0.95	243.5± 7.1	0.25±0.05	-28.5±1.1	76.3	0.0363
TT1-HSA	1.27	278.4± 9.6	0.27±0.07	-31.3±1.15	78.2	0.0499

Table S3: Stability of Pc4 loaded HSA NPs for 6 weeks kept in 4°C determined by the hydrodynamic diameter and the polydispersity index (PDI) measured in DLS and Pc4 release measured by the fluorescence

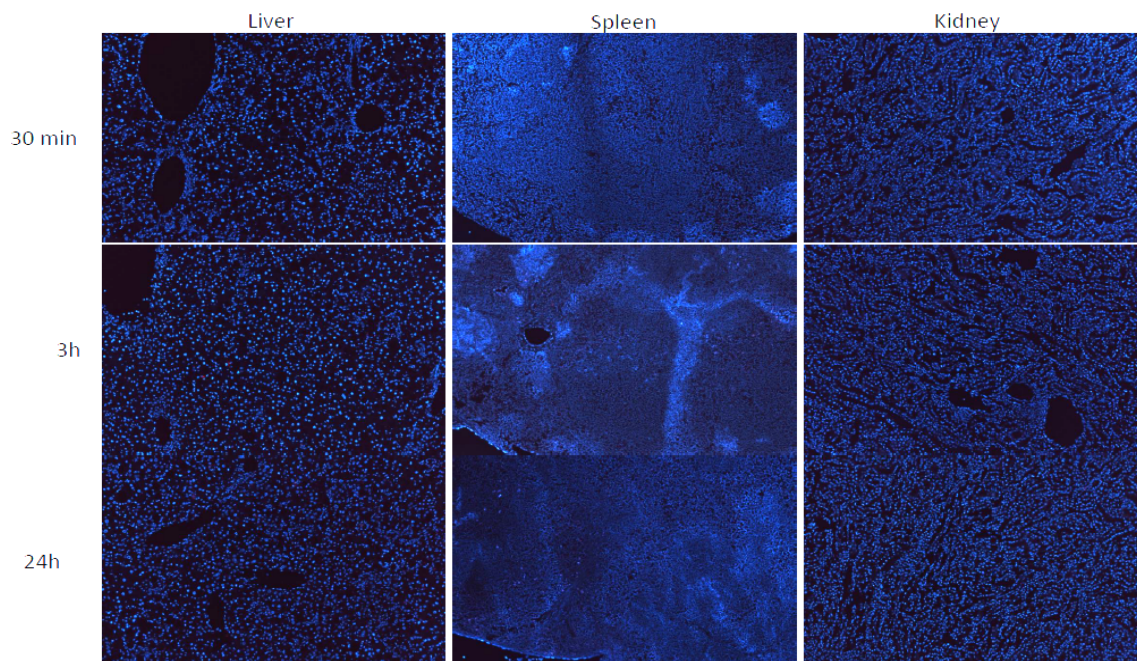
TIME IN WEEKS	Z-AVG HYDROYNAMIC DIAMETER (nm)	PDI	% Pc4 RELEASE
1	248.3 ± 5.3	0.197 ± 0.02	no release
2	269.3 ± 4.3	0.165 ± 0.07	no release
3	268.3 ± 5.6	0.292 ± 0.01	no release
4	221.5 ± 2.6	0.201 ± 0.02	0.8
6	193.6 ± 2.1	0.266 ± 0.01	4.45

Table S4: Stability of TT1 loaded HSA NPs for 6 weeks kept in 4°C determined by the hydrodynamic diameter and the polydispersity index (PDI) measured in DLS and Pc4 release measured by fluorescence

TIME IN WEEKS	Z-AVG HYDROYNAMIC DIAMETER (nm)	PDI	% TT1 RELEASE
1	203.3 ± 7.14	0.147 ± 0.056	no release
2	322.9 ± 20.99	0.204 ± 0.041	no release
3	227.9 ± 19.79	0.298 ± 0.124	no release
4	367.0 ± 15.30	0.237 ± 0.047	9.03
6	313.4 ± 28.77	0.439 ± 0.292	36.13



**Figure S1.** Cellular uptake and localisation study in RAW264.7 macrophage cells. Images were acquired at 30 mins, 2 h, 4 h and 24 h after incubation with (A) Pc4-HSA NPs (0.2 mg/mL) or (B) TT1-HSA NPs (0.2 mg/mL).



**Figure S2.** Nanoparticle distribution in different organs such as liver, spleen and kidney at different timepoints 30 mins, 3 h and 24h after injection in an arteriosclerotic mouse